No. 100, November 2002

SMHI

Reports Meteorology and Climatology

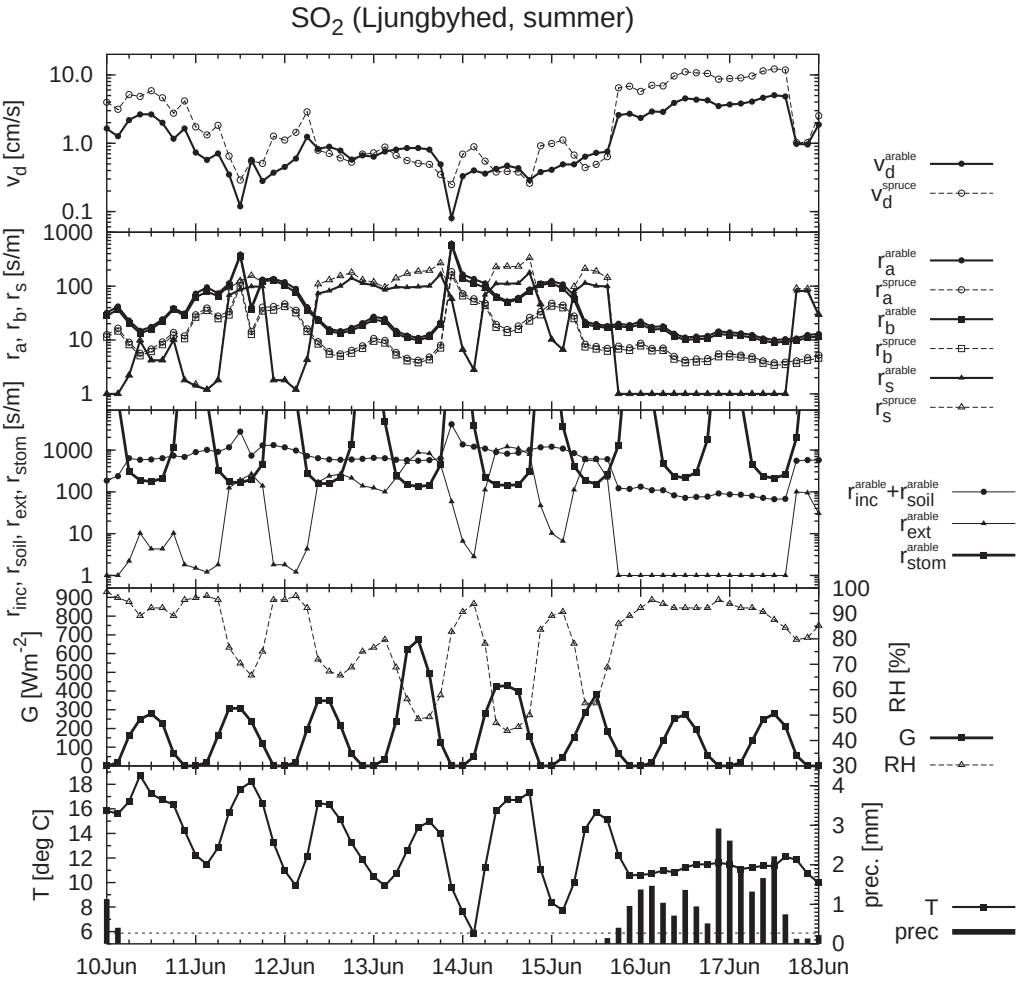

Parameterization of dry deposition in MATCH

Thomas Klein, Robert Bergström and Christer Persson
Swedish Meteorological and Hydrological Institute (SMHI)

RMK
No. 100, November 2002

Parameterization of dry deposition in MATCH

Thomas Klein, Robert Bergström and Christer Persson
Swedish Meteorological and Hydrological Institute (SMHI)

Report Summary / Rapportsammanfattning

Issuing Agency/Utgivare

Swedish Meteorological and Hydrological Institute

S-601 76 NORRKÖPING
Sweden

Report number/Publikation

RMK No. 100

Report date/Utgivningsdatum

November 2002

Author (s)/Författare

Thomas Klein, Robert Bergström and Christer Persson (SMHI)

Title (and Subtitle/Titel

Parameterization of dry deposition in MATCH

Abstract/Sammandrag

The present report describes the calculation of dry deposition in the Multi-scale Atmospheric Transport and Chemistry modeling system (MATCH) applied in environmental monitoring studies. For this type of applications dry deposition is parameterized by means of a resistance concept. Modeled dry deposition velocities for different surface types, a variety of meteorological conditions and several chemical species are presented. The deposition's dependence on the individual partial resistances and their variation with the meteorological conditions are illustrated by means of time-series. The details of the resistance concept are discussed in a pedagogical way in order to both facilitate understanding and to point out different deposition paths.

Sensitivity studies have been performed for the laminar sub-layer resistance of particles for which two different settings of resistance values are compared. The importance of SO_2 and NO_2 uptake by the stomata of plants and the deposition of SO_2 to the external parts of plants have also been investigated by means of sensitivity studies. In addition, horizontal maps and monthly mean values of dry deposition velocities based on meteorological data for 1998 are presented.

Key words/sök-, nyckelord

Dry deposition, resistance concept, NO_2, SO_2, stomata resistance

Supplementary notes/Tillägg

Number of pages/Antal sidor

45

Language/Språk

English

ISSN and title/ISSN och title

0347-2116 SMHI Reports Meteorology Climatology

Report available from/Rapporten kan köpas från:

SMHI
S-601 76 NORRKÖPING
Sweden

Contents

Cover:

Simulated deposition velocities and resistances of SO_2 over arable and spruce and meteorological near-surface variables at the location Ljungbyhed in southern Sweden during a period of summer 1998.

PARAMETERIZATION OF DRY DEPOSITION IN MATCH

1 Introduction

The reliable estimation of the deposition of chemical pollutants over different types of surfaces is of tremendous importance for many ecological and economical decisions. Compounds of sulfur and reduced and oxidized nitrogen can lead to acidification of soils and surface waters. In addition, eutrophication by nitrogen compounds can be a significant environmental problem. Furthermore, the deposition process is important in the context of climate since it can represent an important sink for climatological relevant gases or particles.

Two different types of deposition are generally distinguished in numerical dispersion models. Wet deposition or wet scavenging is the process of atmospheric pollutant removal by means of hydrometeors (i.e. rain, fog or snow). The second way of pollutant transport from the atmosphere to the Earth's surface is known as dry deposition. The latter type of deposition is generally more difficult to describe in numerical models, since it depends on characteristics of the depositing species, properties of the respective surface and the actual meteorological conditions.

The present report describes the calculation of dry deposition in the Multi-scale Atmospheric Transport and Chemistry model system (MATCH) developed at the Swedish Meteorological Institute (SMHI) in Norrköping. MATCH can be applied for a variety of environmental studies. Dry deposition is often parameterized in MATCH by means of a resistance concept. Modeled dry deposition velocities for different surface types, a variety of meteorological conditions and several chemical species are discussed. The investigation illustrates the deposition's dependence on the individual partial resistances and their variation with the meteorological conditions. For particles two different settings of resistance values are compared. The importance of pollutant uptake by the stomata of plants and the deposition of SO_2 to the external parts of plants are further investigated by means of sensitivity studies.

The outline of the present report is as follows: Section 2 provides a description of MATCH with a focus on the parameterization of the dry deposition velocity. In Section 3 the results of MATCH simulations of dry deposition velocities are discussed. The first part of that section is a descriptive review of individual dry deposition processes by means of time series. Sensitivity studies are used to outline the main deposition paths of NO_2 and SO_2. In the second part of Section 3 horizontal maps and monthly mean values of dry deposition velocities based on meteorological data for 1998 are presented. Finally, conclusions are provided in Section 4.

2 Model description

2.1 A summary of MATCH characteristics

The domain of MATCH used in the present study and for, e.g., assessment studies of the environment in Sweden [Persson et al. (1996, 2000)] is shown in Figure 1. MATCH is a three-dimensional Eulerian model comprising a number of modules that can be used for the solution of different individual tasks or combinations of the latter. MATCH is mainly applied to the following three problems:

- modeling of the transport of tracers
- modeling of chemical processes of a variety of species
- modeling of the deposition of species to a receptor surface (ground).

A detailed description of MATCH can be found in Robertson et al. (1999). For completeness, a summary of important MATCH characteristics is presented in Table 1. One major task is the solution of the advection diffusion equation. In order to be more independent MATCH comprises an additional boundary layer package for the modeling of parameters not explicitly provided by the driving model. The MATCH chemistry is based on the EMEP Eulerian acid deposition model chemistry [e.g., Jakobsen et al. (1996), Jonson and Berge (1995), Bartnicki et al. (2001) and references therein].

Table 1: A list of MATCH features and parameterizations.

A summary of MATCH characteristics (Sweden-model)	
advection	Bott (1989a, 1998b, 1992), Robertson et al. (1999)
boundary layer	Robertson et al. (1999); bulk Richardson number approach [Holtslag et al. (1995)]
dry deposition	resistance model (see Section 2.2)
wet scavenging	Langner et al. (1998)
radiation	Josefsson (1989), Langner et al. (1998)
emissions	Gaussian plume model (Berkowicz et al., 1986)
chemistry	e.g., Jakobsen et al. (1995), Jonson and Berge (1995), Bartnicki et al. (2001)
meteorological data	HIRLAM (Källén, 1996), MESAN [Häggmark et al. (2000); see also Section 2.3]

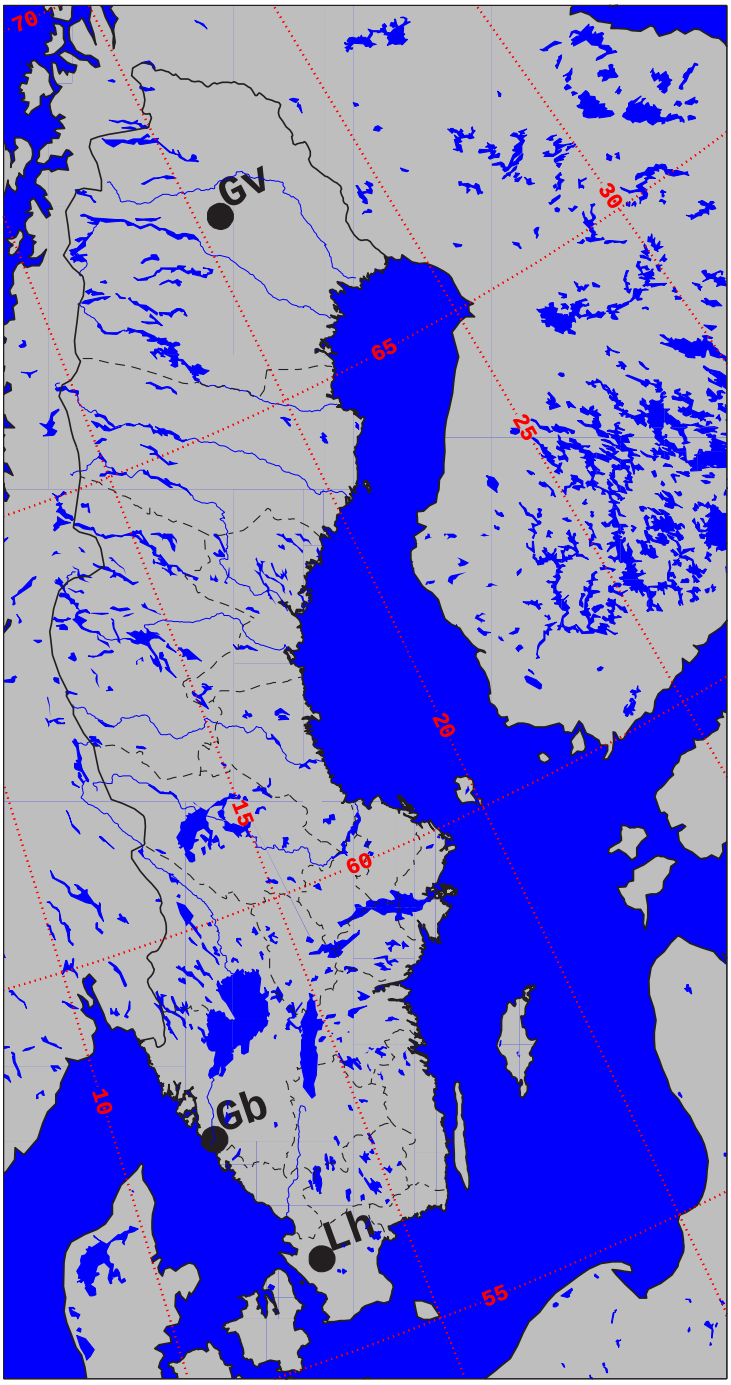

Figure 1: Map of Sweden covering the domain of the Sweden-model version of MATCH. The filled circles labeled Gb, Lh, and Gv indicate the locations of Gothenburg, Ljungbyhed and Gällivare, respectively. The boundaries of Swedish counties are dashed, while the full line marks the borders to Norway and Finland, respectively. Major lakes and rivers as well as sea areas are shown in blue, land surfaces are shaded gray. Latitudes and longitudes are plotted in red with intervals of 5 degrees (dotted).

2.2 Calculation of the dry deposition velocity

The deposition of contaminants (particles, gases) is often parameterized by a resistance concept (e.g. Chamberlain and Chadwick, 1965) in analogy to electrical engineering. The dry deposition flux F_i of a quantity i at height z is determined by its actual concentration $C_i(z)$ and its resistance to transport:

$$F_i(z) = C_i(z) \cdot \frac{1}{r_i(z)} \qquad (1.)$$

In Equation 1 it is assumed that the surface concentration $C_i(z_s)$ is equal to zero. If the latter condition is not given, the difference $C_i(z) - C_i(z_s)$ instead of $C_i(z)$ has to be used[1].

In the electrical resistance analogy the flux F_i corresponds to an electrical current, while the quotient $1/r_i$ represents the conductivity (compare Ohm's law). Physically, the dry deposition process covers three steps. The first step comprises the transport from the free atmosphere through the planetary boundary layer (PBL) towards the laminar sub-layer (the lowest few mm of air close to a surface or an obstacle). The pollutant then has to be transported through the latter layer before it can interact with the respective surface. These three transport processes are parameterized by means of the aerodynamic resistance r_a, the viscous sub-layer resistance r_b and the surface resistance r_s, respectively. The reciprocal value of the sum of these three resistances, which are placed in series, is called the dry deposition velocity and is given by

$$v_d = \frac{1}{r_a + r_b + r_s} \qquad (2.)$$

The different resistances can vary in a complicated manner based on the characteristics of the considered species, actual meteorological conditions and the properties of the respective surface. At present, the MATCH modeling system as used in the standard setup for, e.g., assessing and monitoring the state of the environment in Sweden, differentiates a number of different particles and gases as well as a total of ten different surface types (land use classes, Figure 2[2]).

---

[1] The explicit notation of the z-dependence of the variables is hereafter skipped.

[2] As a result of limiting the number of land use classes to 10, the original land use classes were re-classified, i.e. integrated in remaining classes with similar characteristics. This results, e.g., in an unrealistic percentage of the class "urban" in Northern Norway.

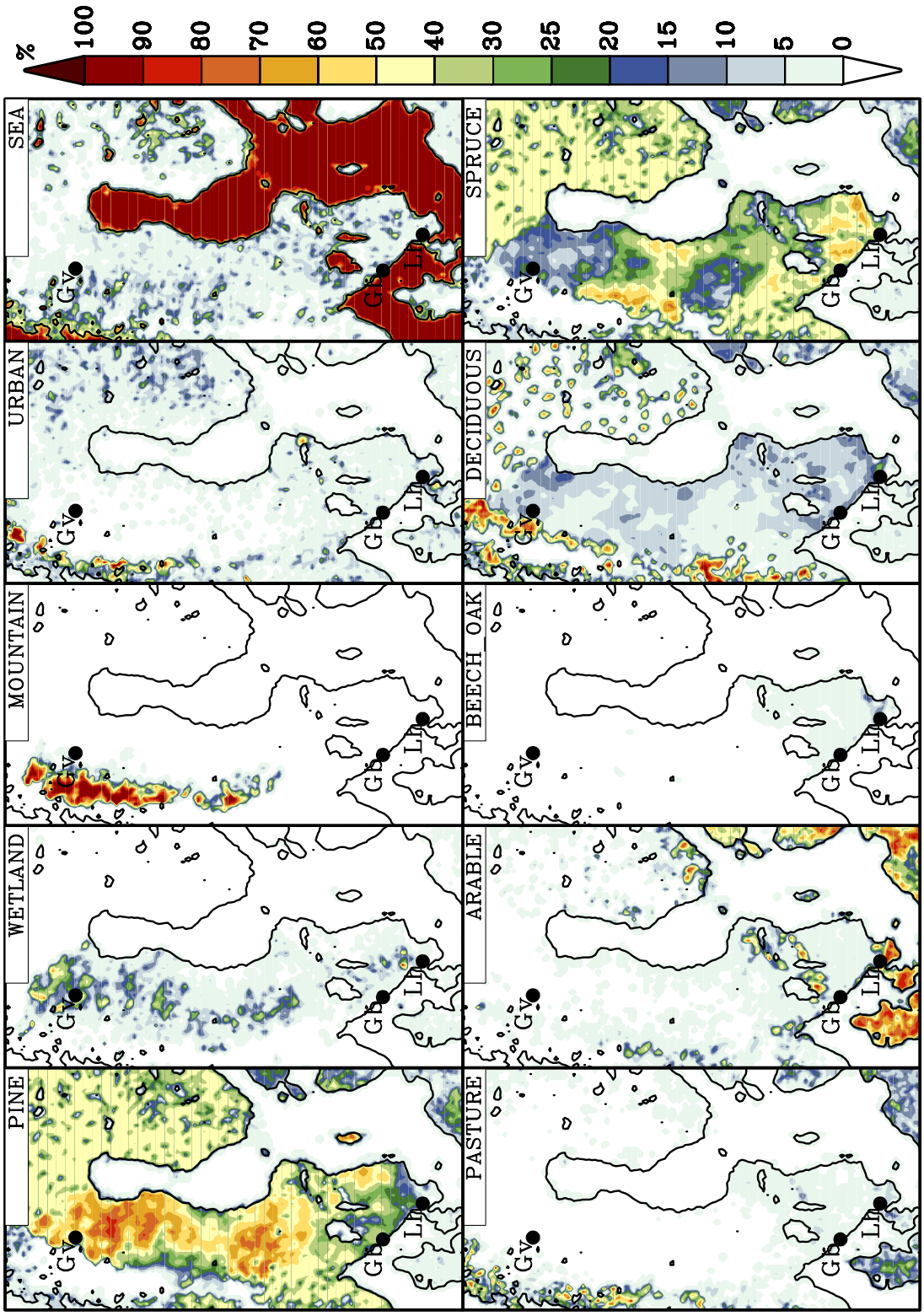

Figure 2. Area coverage in percent of the land use classes used in the standard MATCH version for assessing the environment in Sweden. Lower panel from left to right: pasture, arable, beech/oak, deciduous, spruce. Upper panel from left to right: pine, wetland, mountain, urban, sea. A color bar indicating the respective percentage is shown to the right of the panels. Filled circles labeled Gb, Lh and Gv, respectively mark Gothenburg, Ljungbyhed and Gällivare.

The total dry deposition velocity is obtained as the sum of the area-weighted v_d values obtained for the individual surface classes

$$v_d = \sum_{l=1}^{10} \alpha_l v_{d,l} \qquad (3.)$$

where α_l and $v_{d,l}$[3] are the fractional area coverage and the deposition velocity of the respective surface type *l*, respectively.

The obtained dry deposition velocities can also be adapted vertically by means of similarity theory in order to correspond to the same level as the computed near ground air concentrations. The vertical scaling is performed before the computation of the total deposition velocity (i.e. individually for each class-specific deposition velocity). The deposition velocities presented in this study are valid at a height of 1 m and 1.5 m in the time series and horizontal plots, respectively.

2.2.1 Particles

The resistances for particles are computed or set as described in Table 2 and Table 3. Using a method proposed by Garland (1978), the aerodynamic resistance is calculated according to the actual boundary layer parameters as

$$r_a = \frac{1}{k u_{*l}} \left[\ln\left(\frac{z-d}{z_{0,l}} \right) - \Psi_h\left(\frac{z-d}{L_l} \right) + \Psi_h\left(\frac{z_{0,l}}{L_l} \right) \right] \qquad (4.),$$

where k denotes von Karman's constant and u_{*l} is the friction velocity for the considered land use class *l*. The Monin-Obukhov length (varying for the different land use classes l) and the stability function for heat are denoted by L_l and Ψ_h, respectively. z is the actual height above ground, d the displacement height and $z_{0,l}$ the surface roughness, depending on the land use class *l*. In MATCH, $z_{0,l}$ is assumed to vary according to the season of the year. Table 4 displays the $z_{0,l}$ values used for the different land use classes, while Figure 3 shows the horizontal distribution of the grid-scale roughness height z_0 for the winter and summer season. z_0 is calculated as

$$z_0 = \sum_{l=1}^{10} z_{0,l} \cdot \alpha_l \qquad (5.).$$

[3] In order to avoid long double indices in figures, the notations $v_d^l (\equiv v_{d,l})$ and, e.g., $r_a^l (\equiv r_{a,l})$ are also used for the deposition velocity and the individual resistances hereafter.

Table 2: Computation / setting of resistances for the calculation of the dry deposition velocity of particles in the MATCH model. Numbers in parentheses are viscous sub-layer resistances for the months April to September.

aerodynamic resistance $r_a = \frac{1}{k u_{*l}} \left[\ln\left(\frac{z-d}{z_{0,l}} \right) - \Psi_h\left(\frac{z-d}{L_l} \right) + \Psi_h\left(\frac{z_{0,l}}{L_l} \right) \right]$										
viscous sub-layer resistance r_b [s/m]										
species	pasture	arable	beech oak	deci-duous	spruce	pine	wetland	mountain	urban	sea
$\left\{ \begin{matrix} SO_4^{2-} \\ NO_3^- \\ NH_4 \end{matrix} \right\}$	1000	1000	600 (200)	600 (200)	200	200	800	800	1000	2000
$\left\{ \begin{matrix} Ca^{2+} \\ Mg^{2+} \\ Na^+ \end{matrix} \right\}$	300 (200)	300 (200)	250 (125)	250 (125)	125	125	250	250	250	333
K^+	800 (500)	800 (500)	333 (167)	333 (167)	167	167	333	333	500	1000

Table 3: Alternative set of smaller r_b values (values for summer months in parentheses).

viscous sub-layer resistance r_b [s/m]										
species	pasture	arable	beech oak	deci-duous	spruce	pine	wetland	mountain	urban	sea
$\left\{ \begin{matrix} SO_4^{2-} \\ NO_3^- \\ NH_4 \end{matrix} \right\}$	800 (400)	800 (400)	300 (180)	300 (180)	180	180	800 (400)	800 (400)	500	1000
$\left\{ \begin{matrix} Ca^{2+} \\ Mg^{2+} \\ Na^+ \end{matrix} \right\}$	300 (80)	300 (80)	60 (30)	60 (30)	30	30	250 (125)	250 (125)	250	333
K^+	600 (200)	600 (200)	120 (80)	120 (80)	80	80	600 (300)	600 (300)	600	700

Over large parts of the domain, the grid-scale surface roughness during summer is larger which is a result of the yearly cycle of foliation accounted for in the settings of $z_{0,l}$ for some classes. For the surface class sea the roughness is set directly to the value in Table 4 if the sea is ice-covered (more than 50 % ice coverage). For open sea the roughness is computed in an iterative procedure, taking into account the stress exerted by the near surface winds on the water surface.

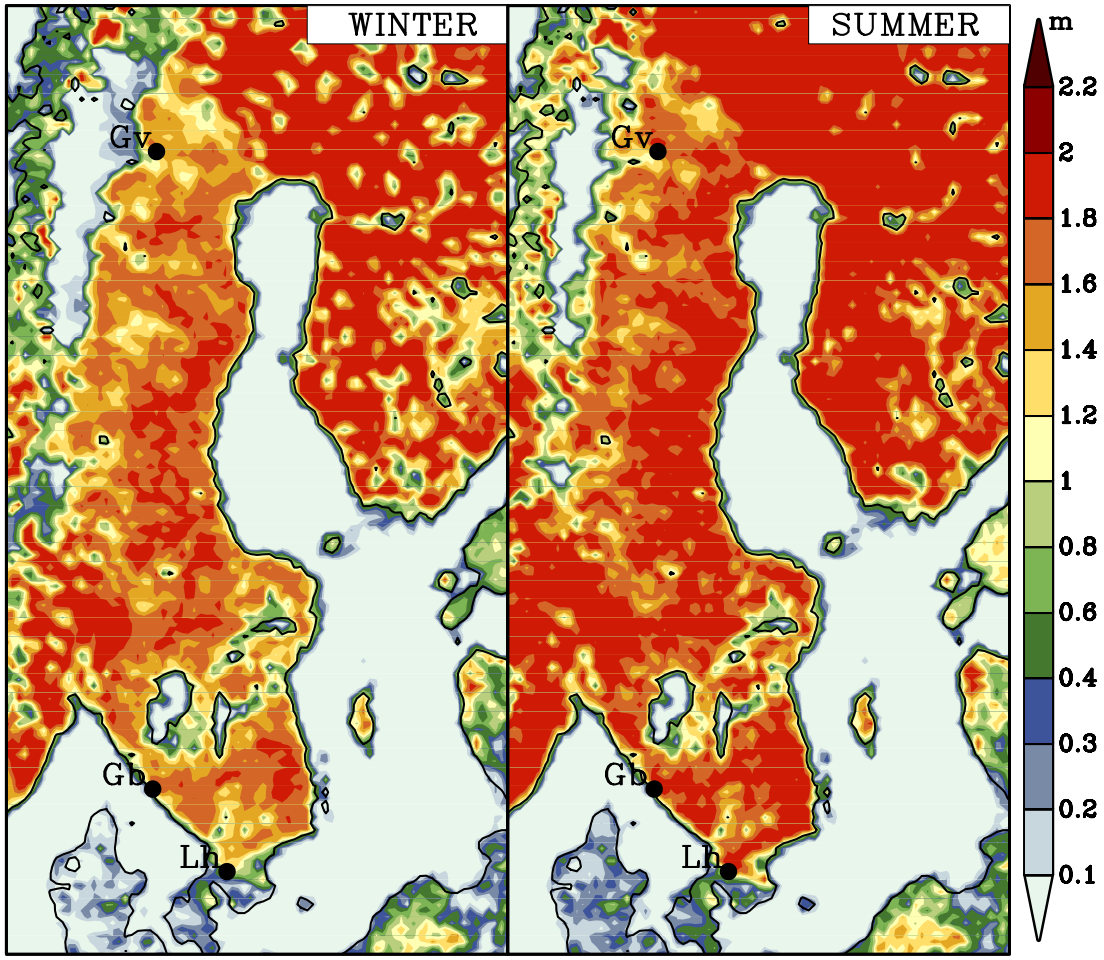

Figure 3. Maps of the grid-scale surface roughness z_0. The left part of the figure shows z_0 values for the winter period (October - March), while z_0 values for summer are displayed in the right part (roughness in m according to the color bar). Filled circles labeled Gb, Lh and Gv, respectively, indicate the positions of Gothenburg, Ljungbyhed and Gällivare on the map.

While the viscous sub-layer resistance is prescribed explicitly, the surface resistance is set to zero. The latter setting is identical with the assumption that the particles adhere the surface. For particles the computation of the deposition velocity therefore reduces to

$$v_d = \frac{1}{r_a + r_b} \qquad (6.)$$

Table 4: z_0-values (m) used for the winter (October – March) and summer (April – September) season in the MATCH calculations.

season	pasture	arable	beech oak	deciduous	spruce	pine	wetland	mountain	urban	sea
Oct – Mar	0.02	0.01	0.5	0.3	2.0	2.0	0.1	0.03	2.0	0.01
Apr – Sep	0.04	0.1	2.0	2.0	2.0	2.0	0.3	0.03	2.0	0.01

In the present version of MATCH, r_b is treated as constant. Two different settings of r_b are discussed in this report. The first setting with relative large values of r_b is shown in Table 2 while the second set with smaller values is listed in Table 3. The values of r_b were chosen to yield reasonable deposition velocities compared to the measurements by Tørseth and Semb (1998) and vary depending on the particles' size and density. For the summer season lower values of r_b are chosen, assuming a reduction of the viscous sub-layer resistance due to the effect of foliation.

For large particles, gravitational settling has to be taken into account, providing a second transport path for pollutants with larger diameter and density. In the framework of the electrical resistance analogy, gravitational settling acts parallel to the transport processes accounted for by $1/(r_a + r_b)$ (see Figure 4).

This process can be accounted for by explicitly prescribing a settling velocity v_s. The deposition velocity for large particles is then given by

$$v_d = \frac{1}{r_a + r_b + r_a\, r_b\, v_s} + v_s \qquad (7.),$$

where the term $r_a\, r_b\, v_s$ represents a virtual resistance (e.g., Seinfeld and Pandis, 1998).

More advanced calculations of gravitational settling rely on Stokes' formula, where v_s is computed depending on the specific particle characteristics like the particle aerodynamic diameter d_p and density ρ_p, the dynamic viscosity of air μ, the gravitational acceleration g and Cunningham's slip correction factor C_c as

$$v_s = \frac{{d_p}^2 \rho_p g C_c}{18\mu} \qquad (8.).$$

Both formulations can be used for MATCH applications, where the process of gravitational settling is assumed to be more important. In the present report, however, v_s is neglected (set to zero) and not discussed any further.

Instead of the treatment of r_b as a constant a newer parameterization based on the work of Zhang et al. (2001) has also recently been implemented in MATCH and is outlined in the Appendix A.

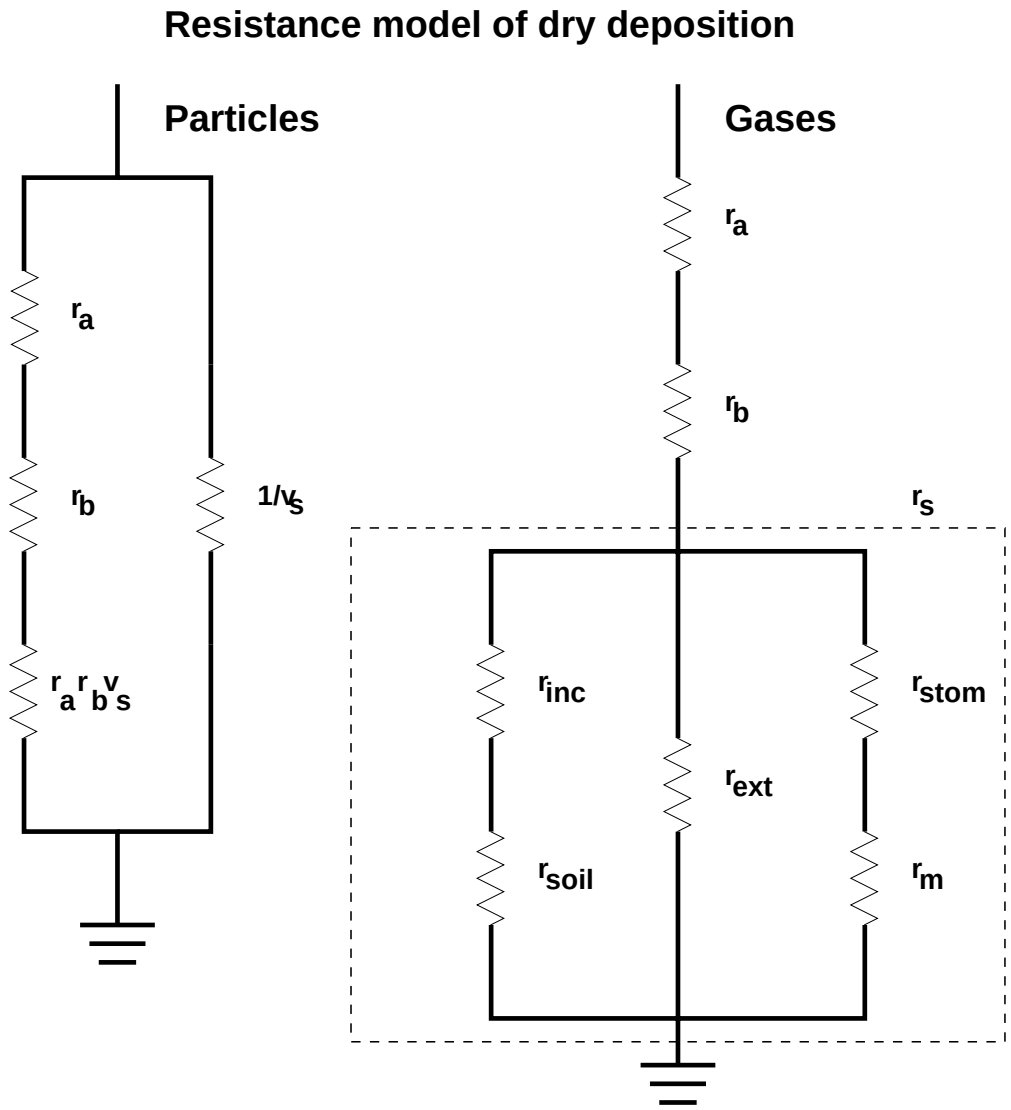

Figure 4. Scheme of the deposition of particles (left part of figure) and gases (right part) using the electrical resistance analogy. r_a, r_b and r_s denote the atmospheric, laminar sub-layer and surface resistance, respectively. r_{inc}, r_{soil}, r_{ext}, r_{stom} and r_m are the in-canopy, soil, external, stomata, and mesophyll resistance, respectively, while v_s denotes the settling velocity. The term $r_a r_b v_s$ is a virtual resistance, which might be neglected if v_s is small.

2.2.2 Gases

The calculation of the dry deposition velocity for gases in MATCH is more complex than for particles. The deposition of gases is mainly based on a review article on deposition parameterization by Erisman et al. (1994) and the parameterization used by EMEP (Co-

operative programme for monitoring and evaluation of the long-range transmissions of air pollutants in Europe) described in, e.g., Bartnicki et al. (2001).

2.2.2.1 r_a and r_b

An overview of the treatment of r_a and r_b of gases in MATCH is presented in Table 5. While the aerodynamic resistance r_a is computed in the same way as for particles, the viscous sub-layer resistance r_b over land surface is a function of the quotient of Schmidt number $Sc = \nu / D_i$ and Prandtl number $Pr = \nu / \kappa$ and the surface roughness, the latter taken into account by ku_{*l}. D_i denotes the molecular diffusivity of component *i,* and κ and ν are the thermal diffusivity and kinematic viscosity of air, respectively. Thus, for land surfaces the formulation

$$r_b = \frac{2}{ku_{*l}} \left(\frac{Sc}{Pr} \right)^{\frac{2}{3}} \qquad (9.)$$

is used [proposed by Hicks et al. (1985, 1987)]. The values of D_i and $(Sc/Pr)^{2/3}$ used in the MATCH simulations are listed in Table 5 for different gases (after Bartnicki et al., 2001).

For open water

$$r_b = \frac{1}{ku_{*l}} \ln \left(\frac{z_{0,sea}}{D_i} ku_{*l} \right) \qquad (10.)$$

is applied [according to Hicks and Liss (1976)].

Table 5: Computation of aerodynamic and viscous sub-layer resistances for gases.

aerodynamic resistance $r_a = \frac{1}{ku_{*l}} \left[\ln \left(\frac{z-d}{z_{0,l}} \right) - \Psi_h \left(\frac{z-d}{L_l} \right) + \Psi_h \left(\frac{z_{0,l}}{L_l} \right) \right]$				
viscous sub-layer resistance r_b				
open (ice-free) water		ice-covered water, land		
$r_b = \frac{1}{ku_{*l}} \ln \left(\frac{z_{0,sea}}{D_i} ku_{*l} \right)$		$r_b = \frac{2}{ku_{*l}} \left(\frac{Sc}{Pr} \right)^{\frac{2}{3}}$		
	SO_2	NO_2	HNO_3	NH_3
D_i	0.11 E-4	0.13 E-4	0.11 E-4	0.21 E-4
$(Sc/Pr)^{2/3}$	1.34	1.19	1.34	0.87

2.2.2.2 r_s

Table 6 provides an overview of the treatment of r_s. For ice-covered surfaces the surface resistance r_s is either set explicitly or (in case of the components HNO_3, SO_2 and NH_3) dependent on the near surface temperature. If the surface is snow-free different constant values are prescribed for ice, open water and urban areas, while the surface resistance of all other surface types is generally computed as a function of five particular resistances. In the latter case, r_s is given by

$$r_s = [(r_{inc} + r_{soil})^{-1} + r_{ext}{}^{-1} + (r_{stom} + r_m)^{-1}]^{-1} \qquad (11.)$$

where the respective resistances are the in-canopy resistance r_{inc}, the soil resistance r_{soil}, the external resistance r_{ext}, the stomata resistance r_{stom} and the mesophyll resistance r_m. It should be noted that the resistances $(r_{inc} + r_{soil}), r_{ext}$ and $(r_{stom} + r_m)$ are placed in parallel. The deposition paths of gases are visualized in Figure 4 by means of the electrical resistance analogy.

Table 6: Computation / setting of the surface resistance (s/m) for gases in MATCH.

<table>
<tr><td colspan="8">surface resistance r_s</td></tr>
<tr><td colspan="8">land /sea ice with snow cover (snow depth exceeding 5 cm)</td></tr>
<tr><td>NO_2</td><td>NO</td><td colspan="2">HNO_3</td><td colspan="2">SO_2, NH_3</td><td colspan="2"></td></tr>
<tr><td rowspan="2">2000</td><td rowspan="2">1.E6</td><td>$T < 268K$</td><td>$T \geq 268K$</td><td>$T < 272K$</td><td>$272K \leq T < 274K$</td><td colspan="2">$T \geq 274K$</td></tr>
<tr><td>50</td><td>10</td><td>500</td><td>$70 \cdot (2 - T + 273.15)$</td><td colspan="2">70</td></tr>
<tr><td colspan="8">no snow cover</td></tr>
<tr><td rowspan="2">chem. comp.</td><td colspan="2">sea</td><td colspan="2">urban</td><td colspan="3">other</td></tr>
<tr><td>sea ice</td><td>open water</td><td>wet</td><td>dry</td><td colspan="3" rowspan="4">$r_s = [(r_{inc} + r_{soil})^{-1} + r_{ext}{}^{-1} + (r_{stom} + r_m)^{-1}]^{-1}$</td></tr>
<tr><td>SO_2, NH_3</td><td>500</td><td>10</td><td>10</td><td>1000</td></tr>
<tr><td>NO_2</td><td>5000</td><td>9999</td><td>9999</td><td>1000</td></tr>
<tr><td>HNO_3</td><td>50</td><td>10</td><td>10</td><td>10</td></tr>
</table>

2.2.2.3 r_{inc}

The in-canopy resistance is parameterized according to Van Pul and Jacobs (1994) as

$$r_{inc} = \frac{b\ LAI\ h}{u_{*l}} \qquad (12.)$$

where LAI denotes the one-sided leaf area index, h is the height of vegetation and b an empirical constant. The product $b\ LAI\ h$ is assumed to vary throughout the year as described in Table 7. The physical concept behind this formulation is that the leaves of plants provide a resistance to the transport of pollutants through the vegetation towards the soil and lower plant parts. Taking into account the yearly cycle of crop growth and foliation (e.g. for land use classes arable and deciduous), r_{inc} is set to a maximum value during the summer months July - August.

Table 7: Computation of the in-canopy resistance for gases in MATCH.

in-canopy resistance $r_{inc} = \frac{b\ LAI\ h}{u_{*l}}$										
$b\ LAI\ h$ (dimensionless)										
month	pasture	arable	beech oak	deciduous	spruce	pine	wetland	mountain	urban	sea
Dec – Mar	0	0	280	280	1400	1400	28	14	0	0
Apr	0	0	280	280	1400	1400	56	56	0	0
May	7	14	560	560	1400	1400	56	56	0	0
Jun	21	42	1120	1120	1400	1400	56	56	0	0
Jul – Aug	35	70	1400	1400	1400	1400	56	56	0	0
Sep	21	42	840	840	1400	1400	56	56	0	0
Oct – Nov	0	0	280	280	1400	1400	56	56	0	0

2.2.2.4 r_{soil}

The resistance of the soil r_{soil} is placed in series with r_{inc}. The soil is considered as wet, if the precipitation (accumulated in the period of a few hours prior to the considered time) exceeds a threshold value of 0.27mm. This distinction is necessary in order to account for the degree of solubility of some pollutants whose deposition can be significantly modified if the surface is wet. Grid areas with surface type “water” are considered ice-covered if the ice cover exceeds

50%. If neither r_{inc} nor r_{soil} is available $r_{inc} + r_{soil} = 10^6$ s/m is set, i.e. no deposition flux along this transport path is allowed. The soil resistances used in MATCH are listed in Table 8. Since information on soil types (i.e., basic/acidic soils) is currently not available in MATCH, the variation of soil characteristics in the domain is not accounted for.

Table 8: Soil resistance (s/m) for gases in MATCH.

soil resistance r_{soil}			
chemical component	$T \leq 273$K	$T > 273$K	
		Wet	dry
NO_2	2000	9999	1000
HNO_3	10	10	10
SO_2	500	10	500
NH_3	500	10	100
NO	1.E6		

2.2.2.5 r_{ext}

The computation of the external resistance r_{ext} is summarized in Table 9. r_{ext} represents the resistance against transport of pollutants to the exterior part of the plants (external leaf uptake) and is also often referred to as the cuticle resistance. r_{ext} of SO_2 is assumed to vary with the near surface relative humidity according to a formula proposed by Erisman et al.(1994)[4] which is depicted in Figure 5. If the leaves of plants are wet as a result of precipitation, an external resistance of $r_{ext} = 1$s/m is set. Below air temperatures of $-1°$C external leaf uptake decreases which is accounted for by an explicit setting of r_{ext} depending on the actual temperature.

Since $r_{ext} = 1$s/m in combination with low values of r_a and r_b (e.g. during large turbulence) can lead to unreasonably large deposition values at model grid scale, a modified version of the Erisman scheme is also discussed in this report, where a lower limit of $r_{ext} = 10$s/m is used.

[4] Note that the parameterization of Erisman et al. (1994) will hereafter be referred to as the ”Erisman scheme”.

Table 9: Computation / setting of the external resistance (s/m) for gases in MATCH.

<table>
<tr><td colspan="6">external resistance r_{ext}</td></tr>
<tr><td colspan="6">no vegetation: 1.E6</td></tr>
<tr><td colspan="6">vegetation:</td></tr>
<tr><td rowspan="3">SO_2</td><td colspan="5">Original Erisman et al. (1994) parameterization:</td></tr>
<tr><td>wet
$r_{ext} = 1\,\mathrm{s/m}$</td><td colspan="2">humid ($RH \geq 81{,}3\%$)
$r_{ext} = 0.58 \cdot 10^{12} \cdot e^{(-0.278 * RH)}$</td><td colspan="2">dry
$r_{ext} = 25000 \cdot e^{(-0.0693 * RH)}$</td></tr>
<tr><td colspan="3">$268.15\mathrm{K} \leq T < 272.15\mathrm{K}$
$r_{ext} = 200\,\mathrm{s/m}$</td><td colspan="2">$T < 268.15\mathrm{K}$
$r_{ext} = 500\,\mathrm{s/m}$</td></tr>
<tr><td colspan="5">Modification of the above scheme (“modified Erisman scheme”):
Same as above but with a lower boundary of $r_{ext} = 10\,\mathrm{s/m}$.</td></tr>
<tr><td>NO</td><td colspan="5">1.E6</td></tr>
<tr><td>HNO_3</td><td colspan="5">10.</td></tr>
<tr><td>NO_2</td><td colspan="2">wet
2000</td><td colspan="3">Dry
1000</td></tr>
<tr><td rowspan="2">NH_3</td><td rowspan="2">$T < 268\mathrm{K}$
500</td><td rowspan="2">$268\mathrm{K} \leq T \leq 272\mathrm{K}$
200</td><td colspan="3">$T > 272\mathrm{K}$</td></tr>
<tr><td>$PAR > 150\,\mathrm{W/m^2}$
2000</td><td colspan="2">$PAR \leq 150\,\mathrm{W/m^2}$
20</td></tr>
</table>

2.2.2.6 r_{stom}

The stomata resistance r_{stom} represents the resistance against the uptake of pollutants by the stomata of plants and is treated according to Wesley (1989):

$$r_{stom} = r_{int} \cdot \left[200/(PAR \cdot 2 + 0.1)\right]^2 \cdot 400/\left[T_C \cdot (40 - T_C) \cdot D_{H_2O}/D_i\right] \qquad (13.).$$

Depending on air temperature (T_C denotes the temperature in degrees Celsius) and photosynthetically active radiation *PAR* (assumed to be half of the global radiation *G)*, the stomata resistance generally decreases significantly during a summer day. Figure 6 demonstrates Wesley’s formula. As soon as the near surface temperature is in a range suitable for photosynthesis (with an optimum temperature of $20^o C$), stomata uptake of pollutants can occur, provided that *PAR* is large enough. Above about $40^o C$ and below $0^o C$ no stomata

uptake is possible. Plant growth and foliation cycles and subsequent variations of the integrated leaf area are associated with variations of the amount of stomata available for stomata uptake. This effect is accounted for by the yearly cycle of the internal resistance r_{int} as denoted in Table 10. The minimum value of r_{stom} is given by $r_{int} \cdot D_{H_2O} / D_i$ (Figure 6a). A comparably large range of temperature and radiation values allows for a relatively small stomata resistance (Figure 6b). Provided that the photosynthetically active radiation is larger than about $200\,\mathrm{Wm}^{-2}$, a closing of a larger fraction of the stomata (i.e. a rapid increase in the stomata resistance) only occurs for comparably low (below about $10^o C$) or large (above about $30^o C$) temperatures. Thus, on a sunny mid-latitude summer day r_{stom} can be expected to be close to its minimum value according to Wesley's formula for a period of several hours.

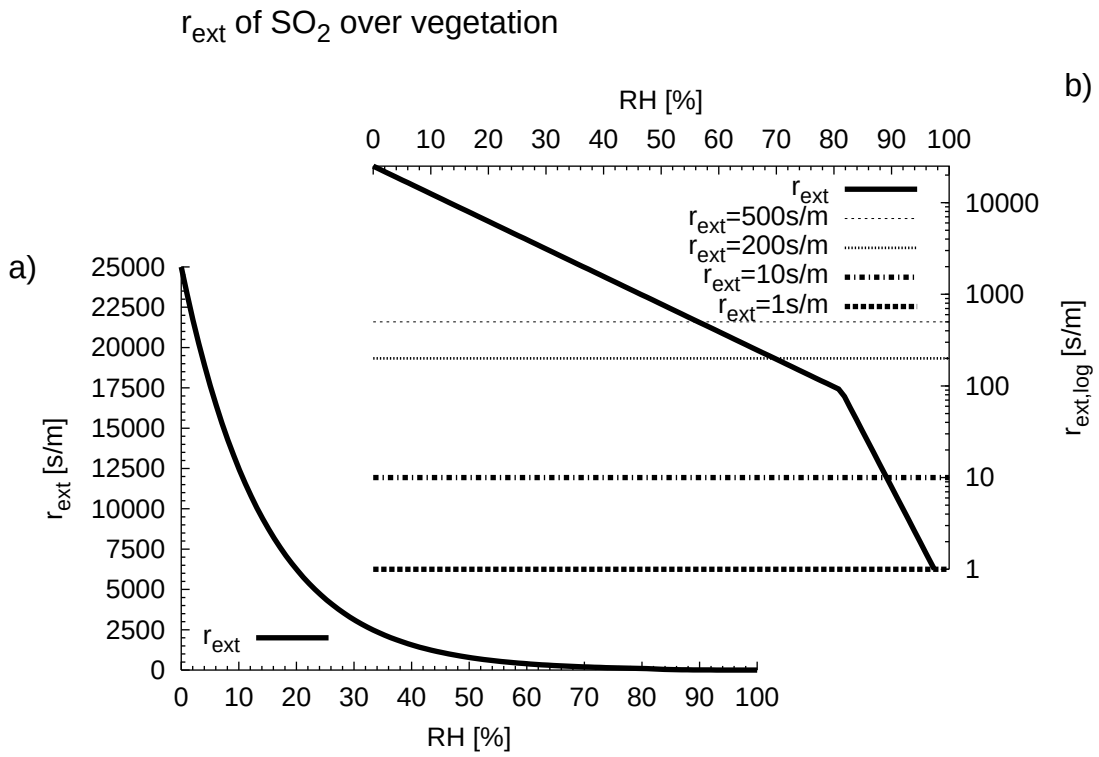

Figure 5. a) Dependence of the external resistance r_{ext} (in s/m) over vegetated surfaces on the near surface relative humidity RH (in %) after Erisman et al. (1994). b) Logarithmic display. For wet surfaces, $r_{ext} = 1\,\mathrm{s/m}$ is used. The settings $r_{ext} = 200\,\mathrm{s/m}$ and $r_{ext} = 500\,\mathrm{s/m}$ are applied if the near surface air temperature is in the range of $268.15\mathrm{K} \le T < 272.15\mathrm{K}$ and $T < 268.15\mathrm{K}$, respectively. In a modified version of the Erisman parameterization $r_{ext} = 10\,\mathrm{s/m}$ is used as a minimum value for r_{ext}.

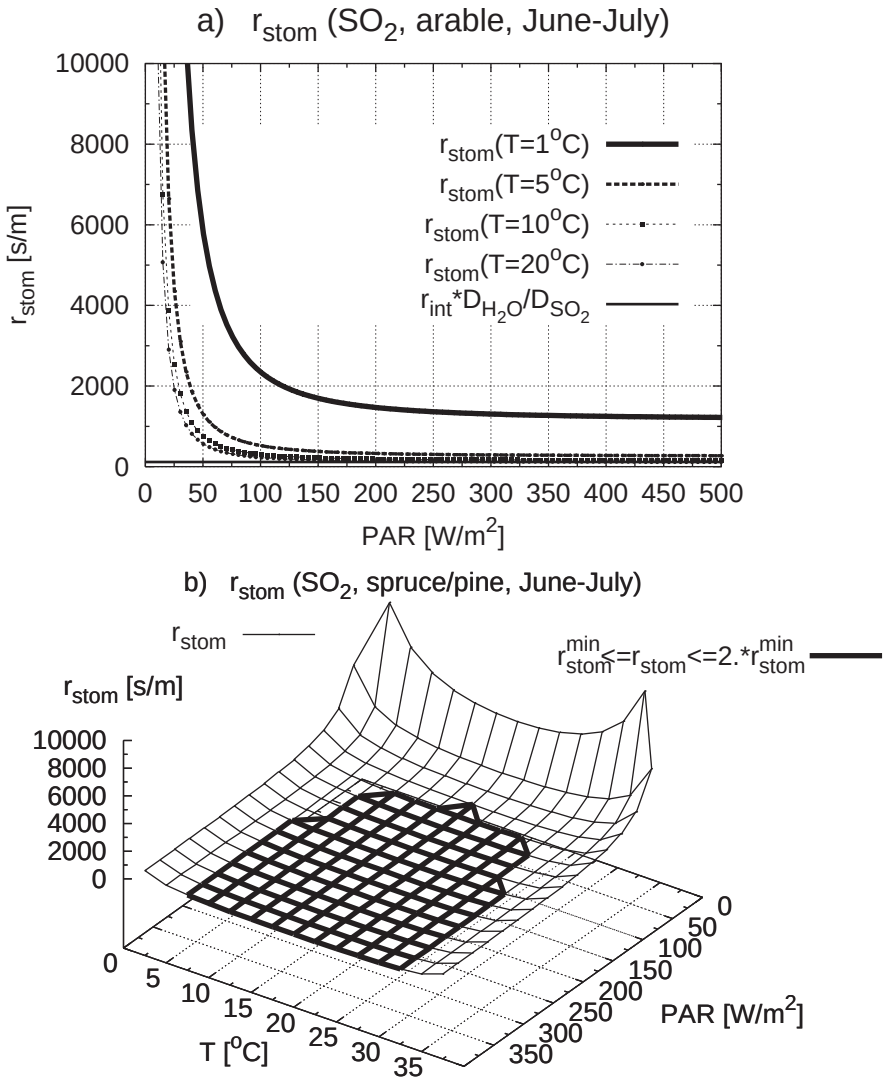

Figure 6. Computation of the stomata resistance after Wesley (1989). a) Variation of r_{stom} with photosynthetically active radiation PAR for different near surface temperatures T, assuming an internal resistance $r_{int} = 60\,\mathrm{s/m}$ (June-July, arable). b) Three-dimensional display of the variation of r_{stom} with T and PAR for spruce/pine ($r_{int} = 130\,\mathrm{s/m}$). The thick lines indicate the area with $r_{stom}^{\min} \le r_{stom} \le 2 \cdot r_{stom}^{\min}$ where $r_{stom}^{\min} = r_{int} \cdot D_{H_2O} / D_{SO_2}$. Note that the variation of r_{stom} with temperature is symmetric about an optimum temperature of $T = 20\,^{\circ}\mathrm{C}$.

Table 10: Calculation of the stomata resistance (all resistances in s/m) in MATCH.

stomata resistance r_{stom}										
no vegetation: $r_{stom} = 1.E6$										
vegetation:										
SO_2, NO_2 (for all other species: $r_{stom} = 1.E6$)										
$273.2K < T < 313.1K$									else	
$r_{stom} = r_{int} \cdot [200/(PAR \cdot 2 + 0.1)]^2 \cdot 400/[T_C \cdot (40 - T_C) \cdot D_{H_2O}/D_i]$									1.E6	
r_{int}										
month	pasture	arable	beech oak	deciduous	spruce	pine	wetland	mountain	urban	sea
Dec – Mar	9999	9999	9999	9999	400	400	800	9999	9999	9999
Apr	9999	9999	9999	9999	250	250	500	9999	9999	9999
May	240	120	140	140	250	250	190	300	9999	9999
Jun – Jul	120	60	70	70	130	130	100	150	9999	9999
Aug – Nov	9999	9999	9999	9999	250	250	500	9999	9999	9999

2.2.2.7 r_m

Current knowledge on the mesophyll resistance r_m is still quite uncertain. Therefore, r_m is assumed to be negligible and set to zero in the present version of MATCH.

2.3 The meteorological data

The meteorological data used to drive the current version of MATCH is a combination of forecasts from the operational HIRLAM version of SMHI (upper air data) and re-analyses of near surface parameters provided by the mesoscale analysis system MESAN (Häggmark et al., 2000). +3h and +6h HIRLAM forecasts and 3-hourly MESAN analyses are used to update the meteorological conditions every 3h. For the present study, HIRLAM results on a grid with 44 km grid spacing are used. Since MESAN applies a grid with 11 km grid spacing, the HIRLAM results are interpolated to the MESAN grid in order to provide a complete set of meteorological variables at 11 km resolution for the MATCH simulations.

Since the dry deposition velocity depends largely on meteorological near surface parameters (wind speed, temperature, global radiation, relative humidity as well as stability parameters), a comparison of observed and MESAN-analysed / MATCH-calculated near surface quantities is shown in Figure 7 for the location Gothenburg at the Swedish west coast. Although the data are not independent, since the observations are also partly used in the MESAN analyses scheme, the comparison is useful to demonstrate the quality of the meteorological input data applied for the MATCH calculations. For both the winter and the spring period shown in Figure 7 the MESAN-analysed parameters wind speed and temperature agree well with the observations provided by an automatic weather station. Furthermore, precipitation analyses also show a qualitatively favourable agreement with the observations. Considering the amount of precipitation it should be noted that MESAN's precipitation is valid at grid-scale and therefore smoothed while the observations are valid at a certain location. Thus, MESAN's precipitation can be expected to be somewhat smaller than the point observations. The reasonable agreement of analysed and observed precipitation is even more important for the calculation of wet deposition, while for the dry deposition this information is only used to determine if the surface is wet. Surface wetness can directly or indirectly modify the deposition of certain pollutants. Some larger differences between MESAN analyses and observations are present for the relative humidity for the spring period, where the analyses apparently overestimate the moisture content of the air.

The global radiation is not directly provided as input data but computed internally in MATCH using a parameterization developed by Josefsson (1989). The extraterrestrial global irradiance G_{ex} is weighted with the total atmospheric transmittance t and a correction factor g_m, describing multiple reflections between earth surface, atmosphere and clouds. The transmittance factor t is a function of the total cloud cover analysed by MESAN. During clear sky conditions some underestimation of the global radiation by the model can be seen (Figure 7). During cloudy periods, however, the radiation is occasionally overestimated. The latter could be a result of, e.g., erroneous total cloud cover analyses or an oversimplification of radiation processes in the parameterization. Yet, despite the relative simplicity of the chosen parameterization, the computed global radiation values are generally in reasonable agreement with the observations.

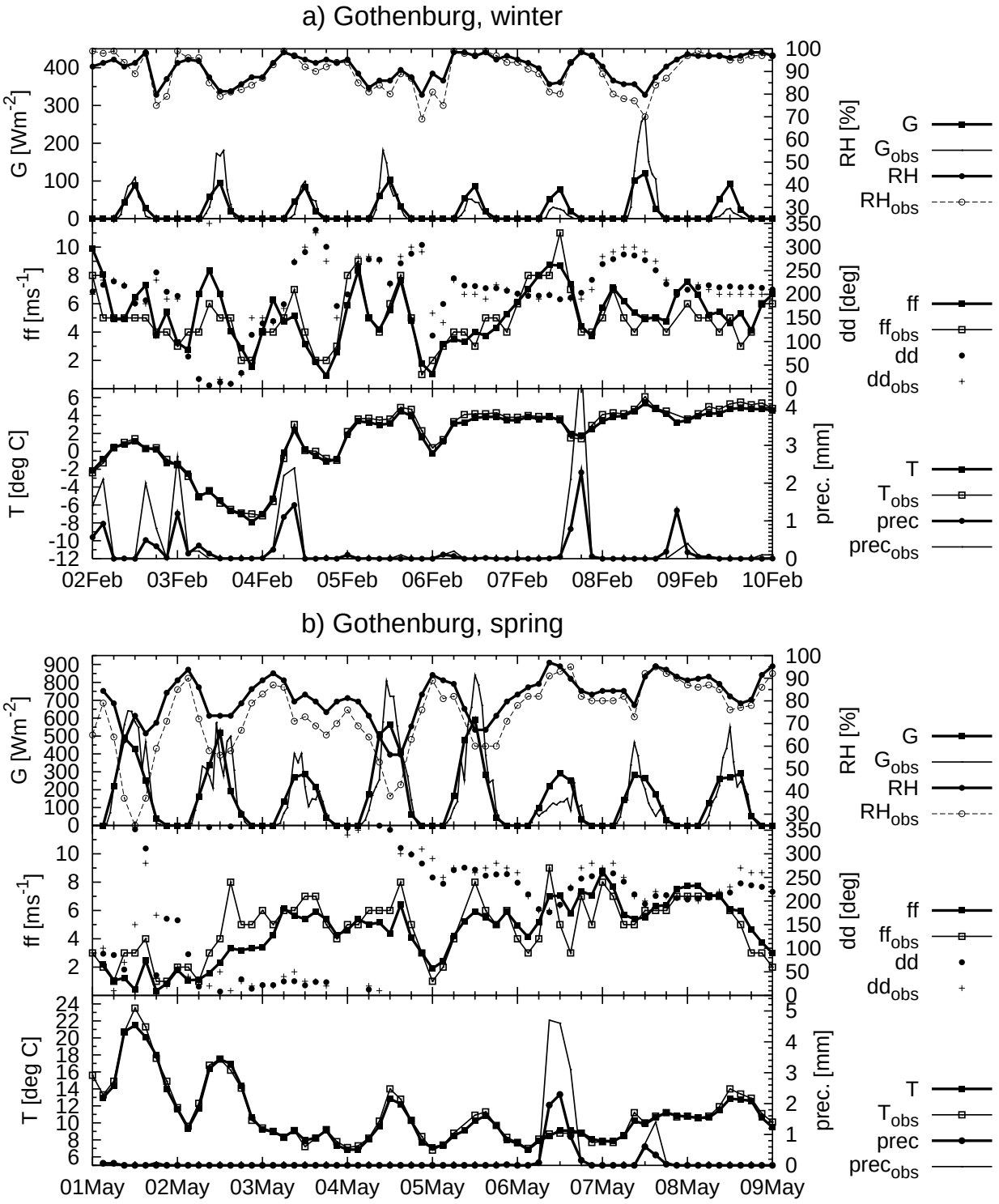

Figure 7. Meteorological parameters used as MATCH input data at Gothenburg (position indicated in Figure 1). MATCH input data is indicated by thick lines with full symbols, while thin lines with open symbols are used to display observational (obs) data from an automatic weather station. a) Example of a winter period (covering 2 - 10 February 1998). Upper panel: global radiation (G, in W/m^2, left y-axis) and relative humidity (RH, in %, right y-axis). Middle panel: wind speed (ff, m/s, left axis) and wind direction (dd, degree, right axis) at 10 m height. Lower panel: temperature at a height of 2m (T, deg. Celsius, left axis) and precipitation (prec, mm, 3h sums, right axis). b) Same as a) but for a spring period (1 - 9 May 1998).

3 Results

In this section examples of MATCH-simulated dry deposition velocities will be discussed. Section 3.1 focuses on the illustration of details of the deposition process and its dependence on the actual meteorological conditions by means of time series at three different locations in Sweden. Since Sweden is to a large degree surrounded by the sea and largely influenced by its presence, the location of Gothenburg at the western coast of Sweden was chosen as one representative example. For the area of southern Sweden, the site Ljungbyhed is presented, while the location of Gällivare is assumed to be representative for the northern parts of Sweden. Representative in this context mainly refers to the meteorological conditions and not necessarily to the extent of individual land use classes, which can vary significantly in most parts of Sweden (compare Figure 2). Yet, the "grid square of Gothenburg" as represented in MATCH, is clearly dominated by the surface types sea (61 %) and urban (29 %), while at Ljungbyhed a large part of the respective area is covered by forest (29 % spruce, 20 % deciduous, 14 % beech/oak) and arable (25 %). The grid area associated with the location Gällivare comprises a small fraction of type urban (6 %), while the larger fractions are forest (44 % pine, 22 % spruce, 11 % deciduous) and wetland (12 %).

In Section 3.2 maps of dry deposition velocities are presented. In addition, mean values of dry deposition velocities for different types of receptor surfaces are discussed.

3.1 Time series of deposition velocities

3.1.1 Ca^{2+}

As a representative species of alkaline particles, Ca^{2+} is discussed in this subsection. Figure 8a shows MATCH-modeled dry deposition velocities, resistances and friction velocities for a week in winter 1998 (2 - 10 February 1998). In general, v_d over both surface categories sea and urban is largely determined by the constant viscous sub-layer resistance r_b, comprising an upper limit of v_d. The variation of v_d, however, is governed by the variable resistance r_a, which in turn is anti-correlated with the friction velocity. This is physically plausible since turbulence is enhanced during windy periods and consequently large values of u_*, leading to an increased transfer of pollutants from the air towards the laminar sub-layer, where Brownian transport becomes the dominating process. For larger particles, gravitational settling provides a second way of transport from the atmosphere to the ground. Note that in the present study this process (although in general implemented in MATCH) is not considered for the presented species, implying the assumption that the particles are sufficiently small.

Comparing the dry deposition velocities over sea and over urban areas, the calculated values differ because of the differences in surface roughness. This effect is explicitly accounted for in the setting of the constant resistances r_b^{sea} and r_b^{urban}. Considering the atmospheric resistance r_a, the smaller roughness of the sea surface leads to smaller friction velocities, i.e.

comparably small turbulence. As a result of the $1/u_*$ dependence of r_a, the dry deposition velocity is strongly correlated with u_*, while the variation of the second term in Equation 4 (Garland, 1978) is relatively small (not displayed).

Although the dry deposition velocity over sea is clearly smaller than over urban areas, its variability is significantly larger. This is a result of r_a^{sea} and r_b^{sea} being of roughly the same order of magnitude (note that in the present parameterization scheme r_a can both exceed or fall below r_b). Consequently, changes in r_a^{sea} have a larger impact on v_d^{sea} than changes in r_a^{urban} have on v_d^{urban}.

As a consequence of using a constant r_b, the dry deposition velocity of particles in MATCH is explicitly limited by the constant value of $1/r_b$ (see Figure 8a). Despite its simplicity this parameterization provides reasonable results. More sophisticated types of parameterization have recently been implemented in MATCH and are currently tested at SMHI (Appendix A).

The importance of the values chosen for r_b is demonstrated in Figure 8b, where the dry deposition velocity and the resistances over spruce are shown for the two different settings listed in Table 2 and Table 3. With a value of $r_b^{spruce} = 125\,\mathrm{s/m}$ v_d^{spruce} is in the range of $0.5\,\mathrm{cm/s} - 0.8\ \mathrm{cm/s}$. For $r_b^{spruce} = 30\,\mathrm{s/m}$ v_d^{spruce} varies between about $1\ \mathrm{cm/s}$ and $3\ \mathrm{cm/s}$. Comparing with the measurements from Tørseth and Semb (1998), the set of smaller r_b values (Table 3) yields more reasonable values and will therefore be applied in MATCH in the future.

3.1.2 NO_2, winter, no snow cover

The discussion of the dry deposition of gases focuses on NO_2 and SO_2, since the parameterization for these species is more sophisticated than for other species, which are at present – partly due to a lack of scientific knowledge - treated in a more simplified manner. Figure 9 shows MATCH simulation results for the dry deposition velocity of NO_2. The same winter period as for particles is considered, but the location Ljungbyhed and the surface types arable and spruce are discussed instead. The treatment of the aerodynamic resistance is the same as for particles. In contrast to particles, r_b of gases is also variable. Both r_a and r_b vary mainly with $1/u_*$ in the way already described in the discussion of Ca^{2+}. For gases r_a is generally larger than r_b.

For NO_2, the surface resistance r_s dominates the dry deposition process. If the precipitation accumulated in a certain time period (in this study 3 hours) prior to the considered time exceeds a limit of 0.27 mm, the surface is considered as wet. As can be seen from Figure 9, surface wetness leads to an even larger value of r_s which is reflected in the modeled dry deposition velocities. The surface wetness has a direct impact on the NO_2 deposition to the external surfaces of plants (external resistance r_{ext}, compare Table 9) and to the soil (soil resistance r_{soil}, see Table 8). If the temperature is below $0°\mathrm{C}$, the soil resistance is not affected by the precipitation events, leading to smaller impacts of the events on the surface resistance and the dry deposition values (e.g. between 00 UTC 2 February to about 06 UTC 4 February).

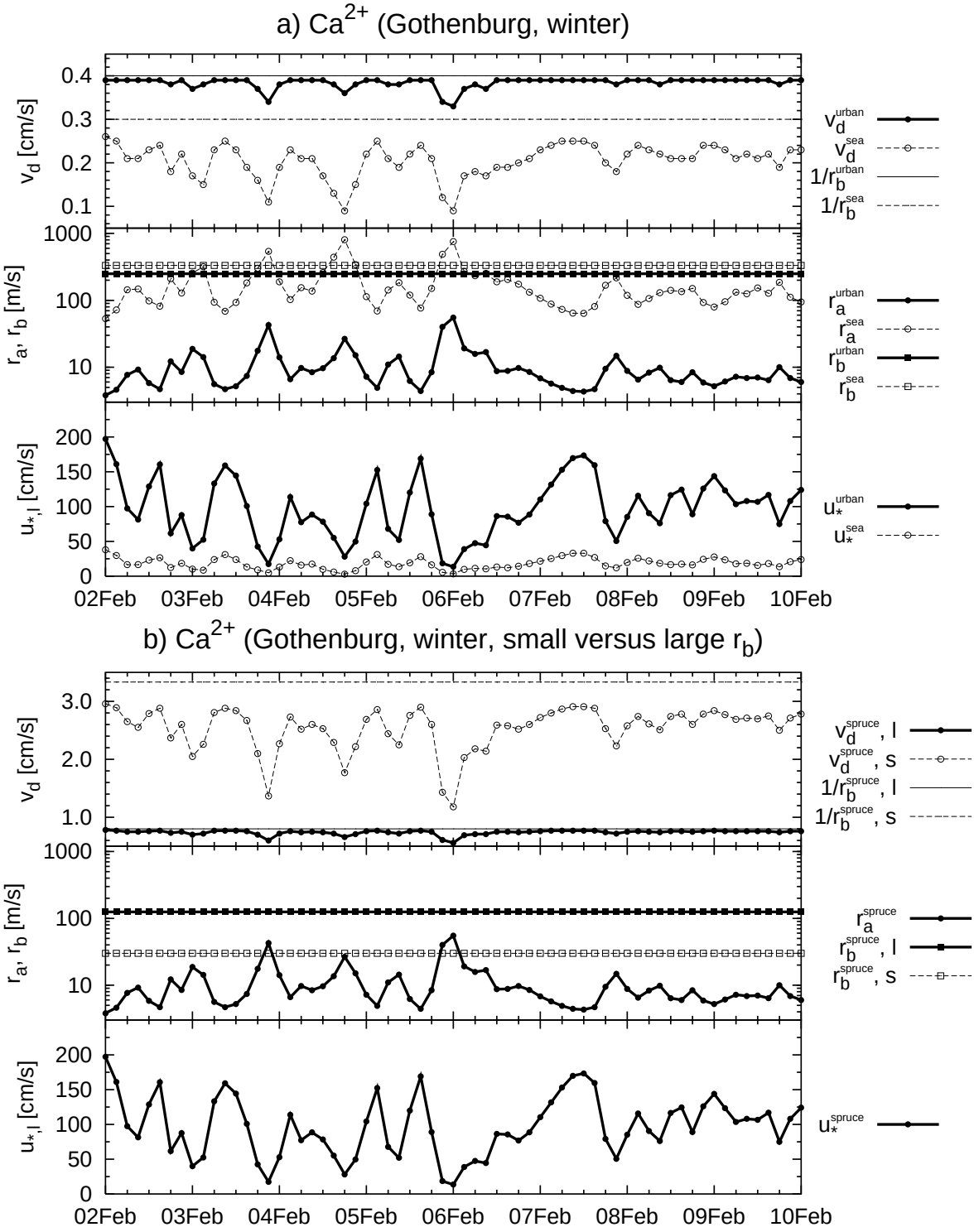

Figure 8. a) Simulated dry deposition velocities of Ca^{2+} (winter period) for the land use classes urban (thick full lines with full symbols) and sea (thin dashed lines with open symbols) at Gothenburg. Upper panel: deposition velocity (v_d, cm/s). The full and the dashed lines without symbols mark the upper limit of v_d for urban and sea which is given by the reciprocal values of the respective laminar sub-layer resistances. Middle panel: atmospheric and laminar sub-layer resistances (r_a and r_b, respectively, both in m/s, r_b values as in Table 2). Lower panel: friction velocity (u_{*l}, cm/s). The plotted resistances and deposition velocities are valid at a height of 1 m. b) Same as a), but for spruce and for large (l) and small (s) r_b values.

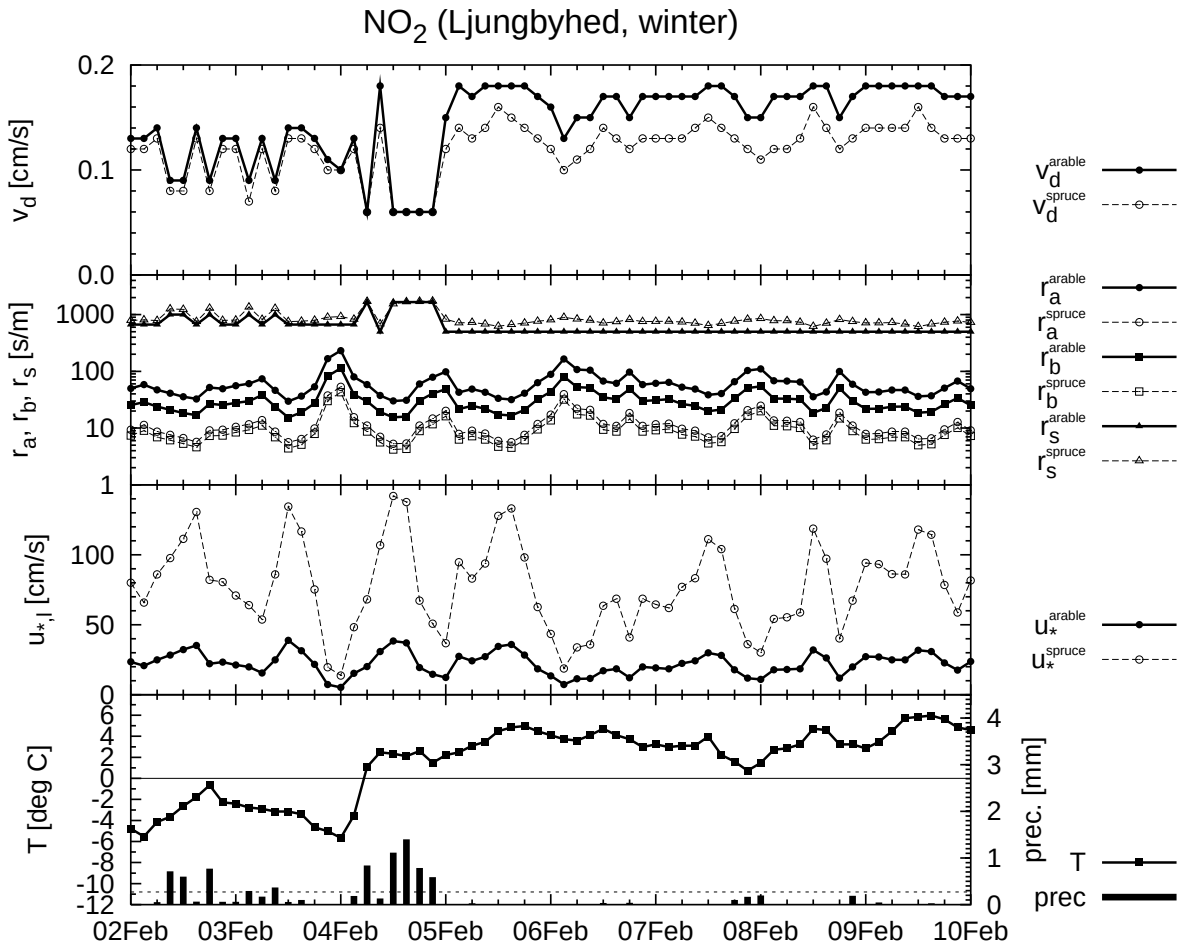

Figure 9 Simulated dry deposition velocities of NO_2 at Ljungbyhed. Upper three panels: same as in Figure 8a, but with the surface resistance (r_s, m/s) added and for the land use classes arable (full thick lines with full symbols) and spruce (thin dashed lines with open symbols), respectively. Lowest panel: MESAN-analysed 2m temperature (°C, full line with full squares) and 3h-precipitation sums (plotted with impulses). The thin dashed line without symbols marks the precipitation limit (0.27 mm) above which the surface is considered as wet. The full line without symbols indicates the 0°C -boundary.

3.1.3 SO_2, winter, no snow cover

For SO_2, the computation of v_d is even more complex than for NO_2, since the surface resistance depends on a highly variable part. According to the formula of Erisman et al. (1994) (see Figure 5 and Table 9), the external resistance of SO_2 varies strongly with the relative humidity. Figure 10 shows modeled dry deposition velocities and resistances for SO_2 as well as meteorological parameters for the same time period as before. With the surface resistance being small, the dry deposition of SO_2 is generally significantly larger (about an order of magnitude) than that of NO_2. Differences in r_a and r_b for the land use classes arable and spruce generally result in large differences of the mean dry deposition to these surfaces. The variability of the dry deposition velocities, however, is mainly governed by the variation of r_s. The variation of r_s, in turn, is a result of the variations of the external resistance r_{ext}. In

contrast to NO_2, precipitation events and subsequent surface wetness favor the deposition of SO_2 to the soil, being accounted for in a low soil resistance of 10 s/m for wet surfaces and temperatures above 0°C (see Table 8). Yet, during precipitation events the leaves of plants are also wet and allow for an efficient uptake of SO_2. The latter is accounted for by an explicit setting of r_{ext} =1s/m in the original scheme of Erisman et al. (1994). The soil resistance is therefore still an order of magnitude larger than the external resistance as can be seen from the precipitation events during the rainy period between 4 and 5 February (Figure 10).

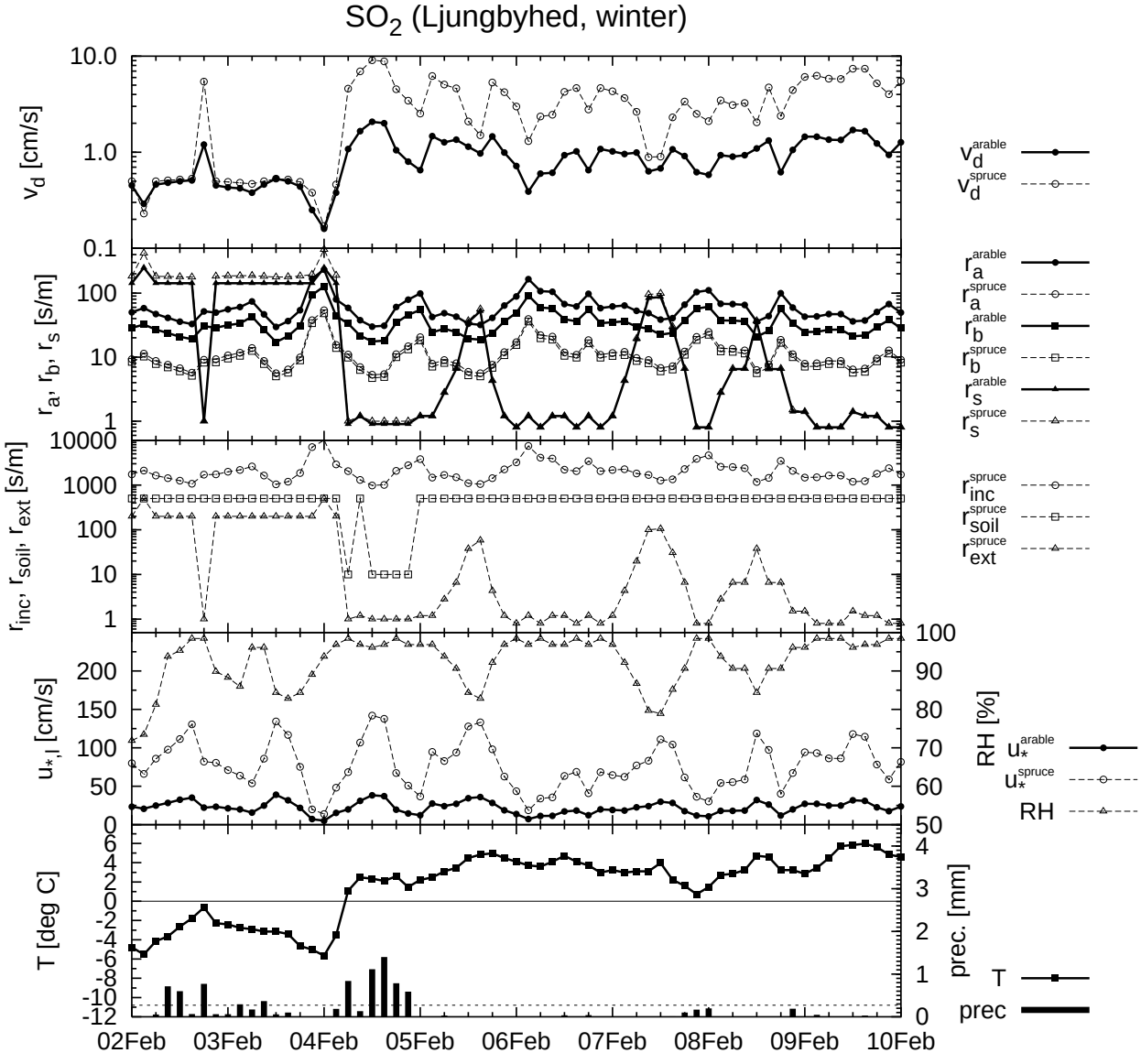

Figure 10. Same as Figure 9, but for the species SO_2. In addition, the individual components of the surface resistance are shown in the second panel from the top, and the relative humidity is included in the lowest but one panel (right axis, in %).

If the near surface air temperature decreases below $-1°C$, the leaf uptake decreases dramatically (see Table 9). Yet, r_{ext} is still smaller or equal to r_{soil}, thereby representing the dominating sink for the pollutant SO_2. The stomata resistance (discussed in more detail in Section 3.1.5) is comparably large during winter and thus the uptake of pollutants by the stomata of plants small. It can therefore be concluded that during winter - according to the present parameterization - SO_2 is primarily deposited to the external of plants. In reality the deposition to the soil can be expected to be much more complicated, and a more sophisticated description of the soil resistance seems necessary which takes the actual soil characteristics (especially soil moisture and pH) into account instead of explicitly prescribing the value of r_{soil}.

In addition, the soil resistance is aligned in series with the in-canopy resistance r_{inc}. For some surface types (e.g. arable, pasture) an annual growth cycle of plants is accounted for in the leaf area index, consequently leading to an annual variation of the in-canopy resistance with $r_{inc} = 0$ during winter. However, for coniferous forest (e.g. spruce as in Figure 10) the in-canopy resistance is large throughout the year, i.e. the deposition path through the canopy towards the soil is nearly closed throughout the year. Taking into account the considerable regional variability of forest characteristics in Sweden (and also many other parts of the world), the presently used derivation of the leaf area index is questionable since it purely differs with land use class. As a consequence, tight forests in e.g. southern parts of Sweden are at present treated in the same way as significantly less tight forests in e.g. the northern areas. This misrepresentation clearly underlines the need for a high resolution map of actual vegetation characteristics in order to better describe both the regional and the annual variation of the in-canopy resistance.

3.1.4 SO_2, winter, snow cover

The surface resistance of SO_2 and NH_3 over ice or snow-covered areas depends on the actual near ground temperature (see Table 6). Figure 11 shows modeled deposition velocities and resistances at Gällivare for a week in March 1998. The grid area of Gällivare is covered by about 10-20 cm of snow during the whole period displayed.

It is obvious that v_d is mainly controlled by r_s. r_s is explicitly set if the temperature exceeds a value of 274 K or falls below 272 K, while a linear relationship is assumed between these boundary values. During the warm episodes a significant increase of v_d by almost an order of magnitude can be noticed over the snow-covered area.

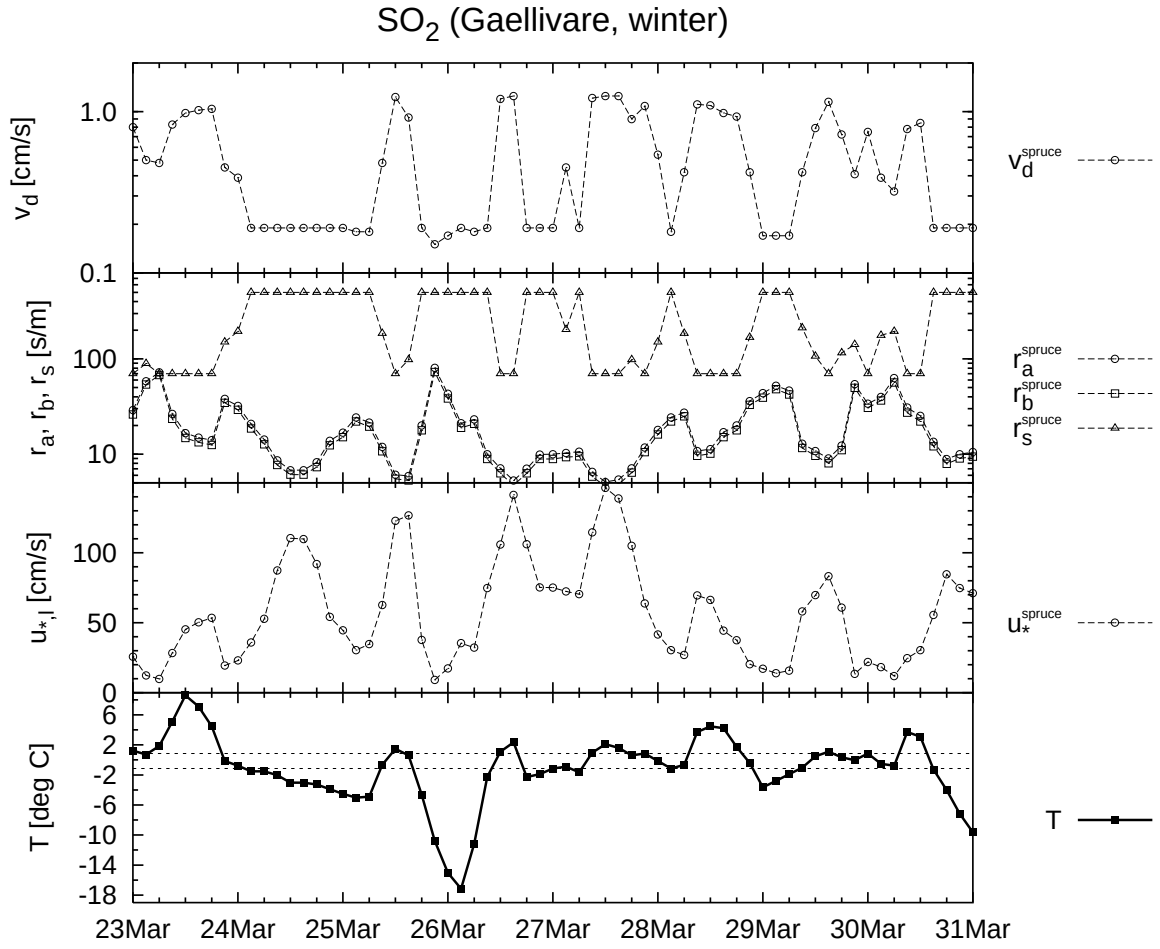

Figure 11: Same as Figure 9, but for SO_2 at Gällivare (location shown in Figure 1) during 23 -31 March 1998 and without land use class arable and precipitation. During the whole period, a snow cover of more than 10 cm was present at Gällivare. For clarency, dashed lines mark the isotherms of 272K and 274K, bordering the range for which a linear relationship of r_s (SO_2, NH_3 and HNO_3) and temperature is assumed.

3.1.5 SO_2, summer

While the previous subsections dealt with the deposition of pollutants under typical winter conditions, this subsection addresses the more complicated deposition process during summer. In addition to the deposition paths discussed previously, the uptake of compounds by the stomata of plants can be significant during a summer day. Figure 12 displays resistances and deposition velocities of SO_2 at Ljungbyhed during a week in summer 1998 (10 – 18 June 1998).

The shown episode is characterized by relatively large variations of r_a and r_b as a result of the meteorological conditions (the friction velocity, not displayed). For those periods during which the relative humidity exceeds about 70%, the external resistance is the lowest of the resistances along the three possible deposition paths, i.e. the pollutant is mainly deposited to the plants' external surfaces.

Yet, during less cloudy conditions the global radiation normally causes a distinct daily cycle of the near surface air temperature. The daily cycle of global radiation and the temperature

cycle are generally slightly out of phase, causing a temperature maximum during the early afternoon. As a consequence of that daily warming, the relative humidity decreases notably during daytime, leading to an increase of r_{ext}. The anti-correlation of temperature and relative humidity and accordingly the correlation of temperature and external resistance are obvious from Figure 12.

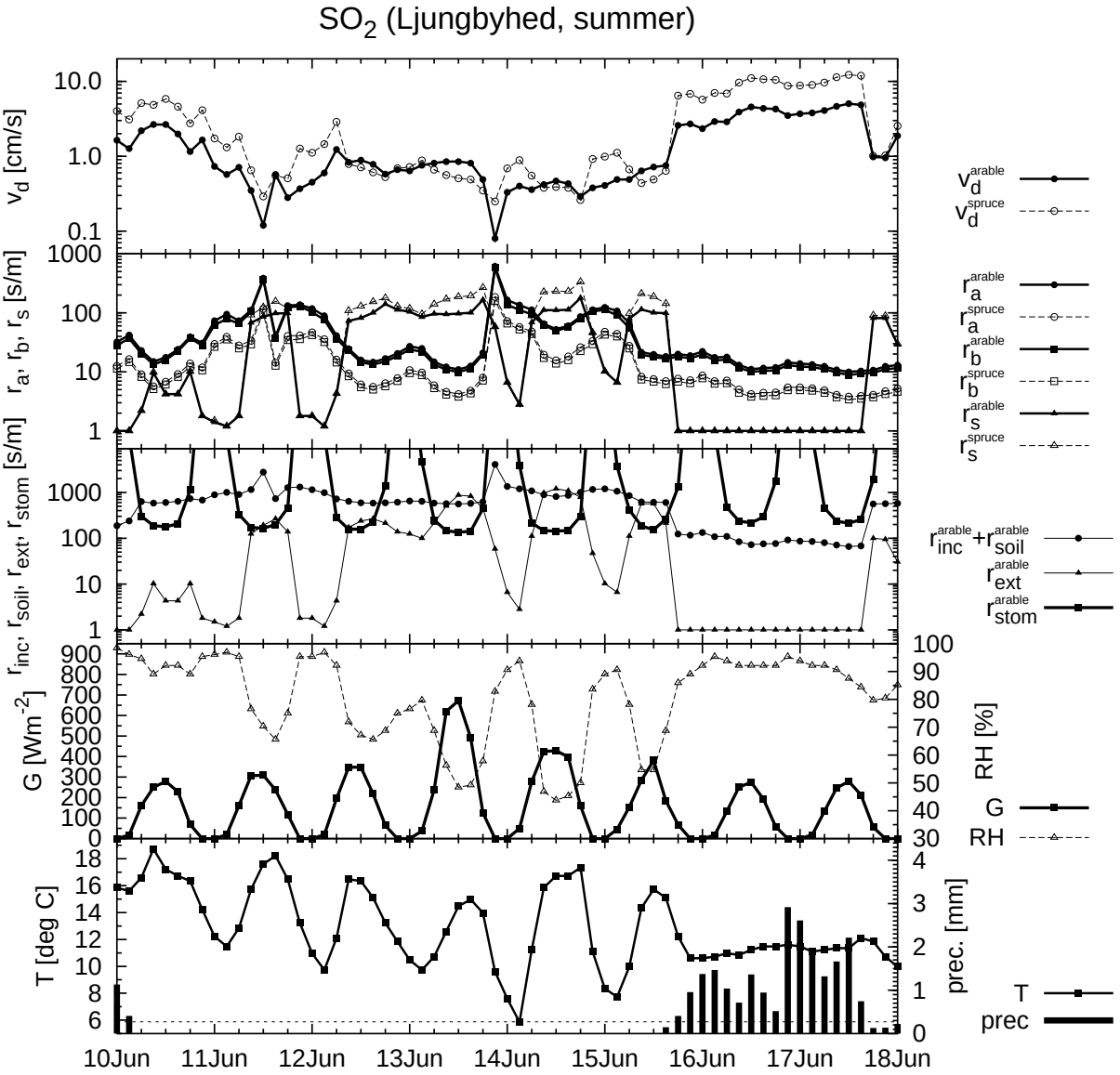

Figure 12: Same as Figure 10, but for a summer period (10 - 18 June 1998). In addition, the global radiation (W/m^2, left axis) instead of the friction velocity is shown on the lowest but one panel, and the middle panel also shows the stomata resistance r_{stom}.

While leading to a warming and drying accompanied by an increase in r_{ext}, the increase of global radiation during daytime also causes an opening of the plants' stomata. The latter in turn causes a considerable reduction of the stomata resistance to the uptake of pollutants. This can be seen by comparing the curves of G and r_{stom} on panels 4 and 3 in Figure 12. For a period of about 6 – 12 hours during daytime, the dry deposition of SO_2 can therefore be

dominated by the stomata's uptake of pollutants. This period is roughly centered at the midpoint between the local solstice and the afternoon near surface temperature maximum.

Considering the land use class arable, a few daytime periods are visible where the stomata resistance r_{stom} actually dominates the deposition process of SO_2. Yet, it is important to note that arable has the lowest internal resistance r_{int}. r_{int} of, e.g., spruce is more than twice as large as r_{int} of arable under summer conditions. Wesley's formula (Equation 13, Table 10) implies that the stomata resistance is limited by a lower boundary value of $r_{int} \cdot D_{H_2O} / D_i$, as is also demonstrated in Figure 6. For coniferous trees like spruce and pine, the minimum value of r_{stom} is therefore comparably large with about $130\,\mathrm{sm}^{-1}$. From Figure 12 it becomes clear that for the latter classes the surface resistance is determined by r_{ext} most of the time. Consequently, the question arises about the importance of the pollutant uptake by the plants' stomata on a larger time-scale, i.e. how many percent of the monthly dry deposition of SO_2 is actually deposited by this mechanism? This aspect is discussed more thoroughly in the following subsection by means of a sensitivity study.

A problem connected to the present formulation of the stomata resistance is its independence of the soil water content. At present, the plants' capacity to absorb pollutants is basically unlimited. However, the surface water content can decrease significantly during a warm summer day and lead to a closure of the stomata. Neglecting this effect in the model can consequently result in a considerable overestimation of pollutant deposition to the stomata of plants. The surface water content is often part of the standard output of numerical weather prediction models. Work is currently underway at SMHI to implement a modified parameterization of the stomata resistance, which also takes into account the availability of surface water.

Due to the differences in surface roughness, z_0, the aerodynamic and viscous sub-layer resistances over arable are normally larger than over spruce (Figure 12). However, the surface resistance over arable is lower than over spruce due to the lower internal resistance and due to the lower $r_{soil} + r_{inc}$. As a consequence, the deposition over spruce is larger than over arable during those periods where $r_a^{arable} + r_b^{arable} - (r_a^{spruce} + r_b^{spruce})$ is larger than $r_s^{spruce} - r_s^{arable}$. This is the case most of the time between 10 and 18 June. Exceptions can be seen between about 9 and 18UTC during the 12-15 June. During these episodes stomata deposition represents the deposition path with the smallest resistance. When stomata uptake dominates, v_d^{arable} can therefore even be larger than v_d^{spruce} because of the lower stomata resistance of arable.

3.1.6 SO_2, sensitivity run without stomata uptake of pollutants

In order to estimate the importance of the stomata uptake of SO_2 during summer conditions, a sensitivity run of the month June 1998 was performed where the stomata resistance was set to 1.E6, i.e. the deposition path via the plants' stomata was closed. Figure 13 shows the deposition velocities obtained in the model run with full deposition parameterization (control run) and the differences between control and sensitivity run in cm/s and in % of v_d for selected land use classes. As was already pointed out in Section 3.1.5, the surface roughness

and consequently the aerodynamic and viscous sub-layer resistances determine the magnitude of the deposition velocity most of the time, causing largest values over forested areas (i.e. spruce and deciduous in Figure 13) and smallest values over mountain regions.

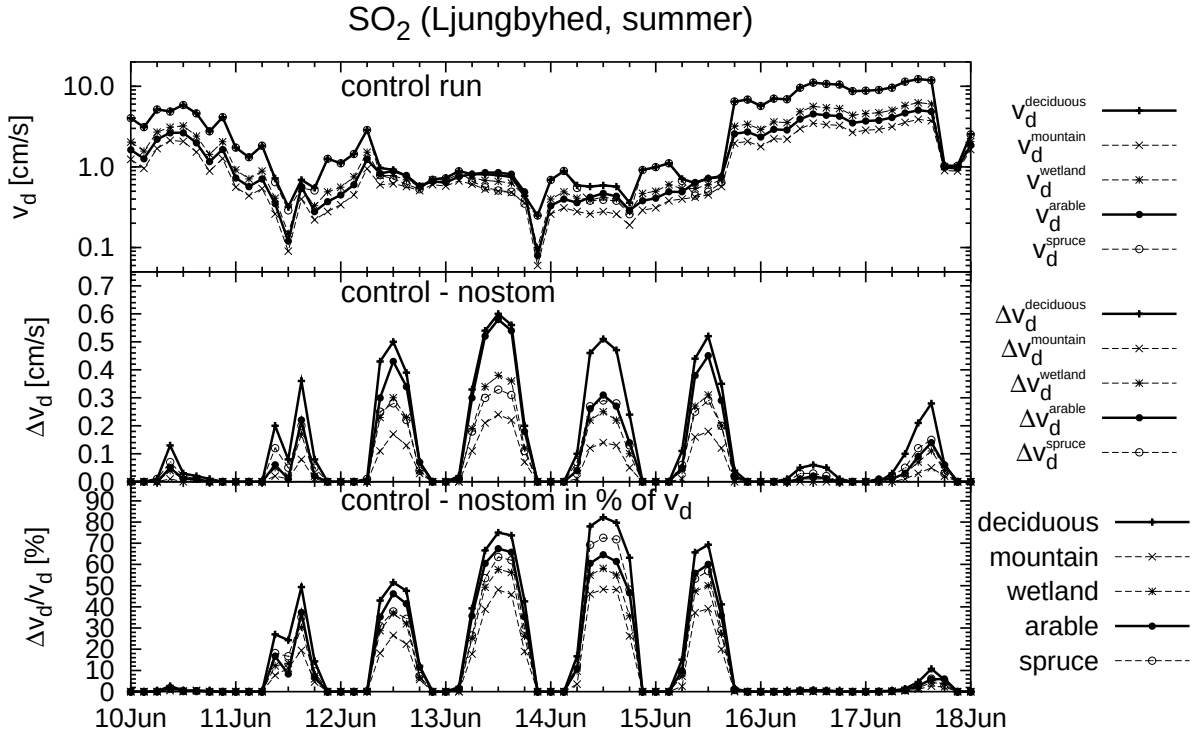

Figure 13: Upper panel: simulated dry deposition velocities for SO_2 at Ljungbyhed during 10 - 18 June 1998 over different land use classes (deciduous, mountain, wetland, arable, spruce) in the simulation with full deposition parameterization ("control run"). Middle panel: differences of the simulated deposition velocities between control run and the simulation without stomata uptake of pollutants (nostom) in cm/s. Lower panel: same as middle panel but in % of $v_d^{control}$.

The largest differences of control and sensitivity run (Δv_d) should generally be expected for arable and deciduous since r_{int} is smallest for these classes. Yet, during certain periods $\Delta v_d{}^{spruce}$ is also surprisingly large, i.e. the stomata resistance is important during these periods. This can, e.g., be a result of the larger roughness length of spruce compared to arable. As a consequence of the more efficient vertical mixing the aerodynamic resistance and the laminar sub-layer resistance are significantly lower than over arable. Thus, even though the change in surface resistance over spruce is smaller than over arable it can have a larger impact on the deposition velocity $v_d{}^{spruce}$. Maximum differences between control and sensitivity run are present for the land use class deciduous with up to 85% of the deposition over that class. The vertical mixing over deciduous is efficient due to the large roughness length while at the same time its internal resistance is comparably low.

3.1.7 SO_2, modified Erisman scheme with a lower boundary of r_{ext}

As can be seen from Figure 12 the modeled dry deposition velocity of SO_2 can reach unreasonably large values of more than 10 cm/s if u_{*l} is large (i.e., during large mechanic turbulence). Therefore, a limit of $r_{ext} = 10\,\mathrm{s/m}$ is used as a lower boundary. This is illustrated by Figure 14 for the summer period of 10 – 18 June 1998.

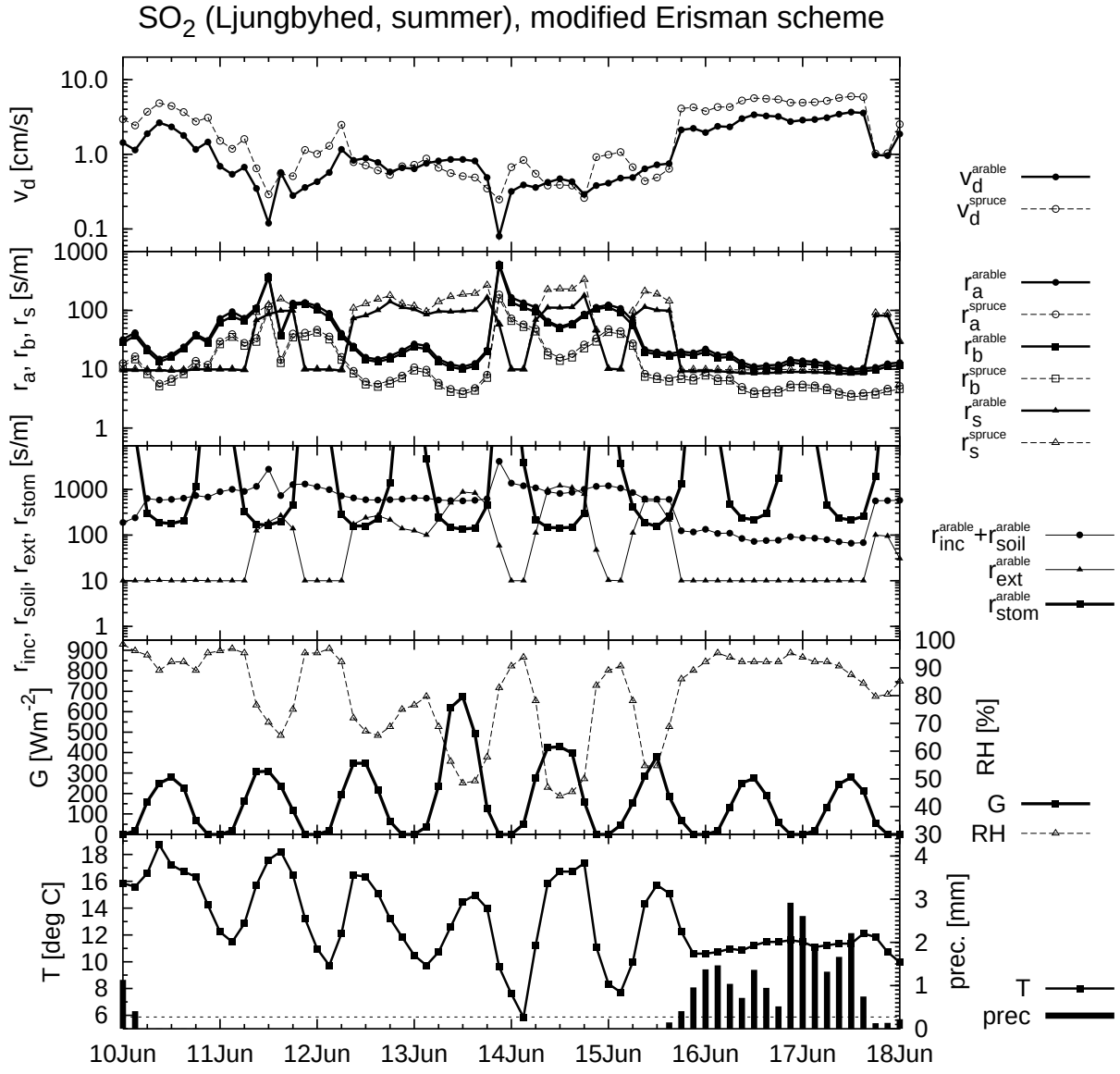

Figure 14: Same as Figure 12, but with the external resistance limited by a lower boundary value of $r_{ext} = 10\,\mathrm{s/m}$.

The differences of the two simulations with the original and the modified Erisman schemes can be seen from Figure 15 for different land use classes. The reduction in deposition velocity can be as large as 50% of the original value in individual cases but is small during most of the time. A sensitivity study with the stomata uptake switched off (not shown) leads to the same

conclusions as pointed out in Section 3.1.6. The stomata uptake of SO_2 can be important during short periods of the day although the major part of pollutant deposition takes place via the cuticles of the plants despite the increased lower limit of r_{ext}.

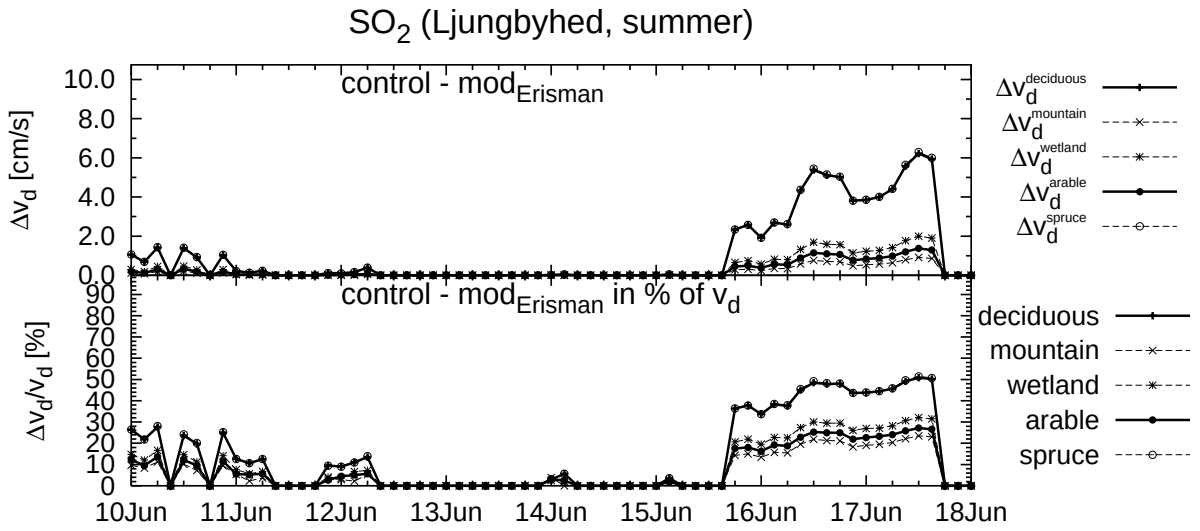

Figure 15: Same as Figure 13, but for the differences between the control run (original Erisman scheme) and the run with a lower limit of $r_{ext} = 10\,\mathrm{sm^{-1}}$ for SO_2 (modified Erisman scheme).

3.2 Monthly mean deposition velocities

In this section simulated monthly mean values of deposition velocities are discussed. Figure 16 shows monthly mean deposition velocities of SO_2, NO_2 and HNO_3 for January and June 1998. v_d of SO_2 and NO_2 shows a pronounced pattern of low deposition in northern Scandinavia in January which results from the large surface resistance over the snow-covered land and sea ice (compare Table 6). For HNO_3 in contrast the deposition velocities are relatively large in that area since the surface resistance is set to the comparably low value of $r_s = 50\,\mathrm{sm^{-1}}$ over snow. Therefore, variations in r_a and r_b have a larger impact, causing significant variations of v_d even over the snow-covered areas.

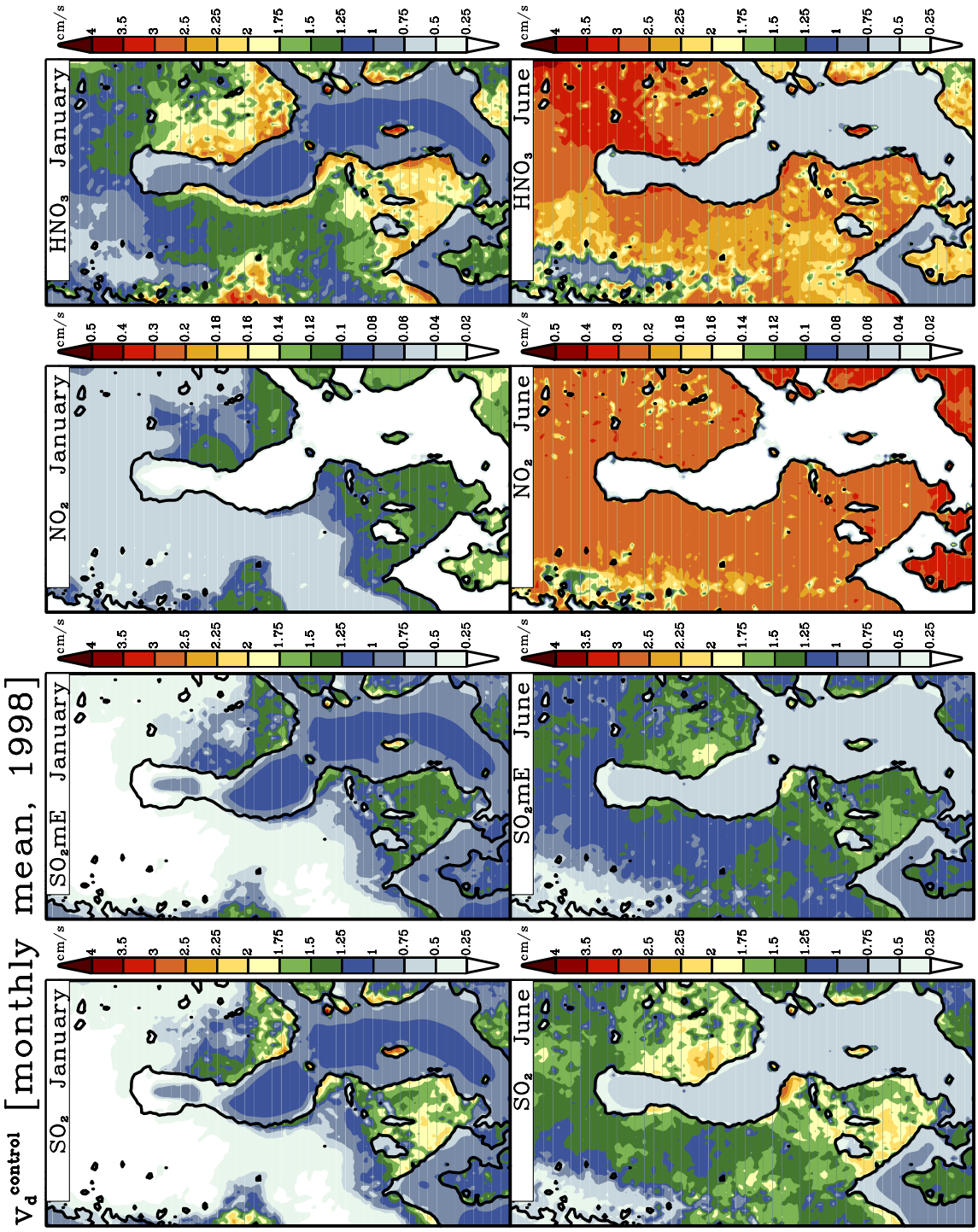

Figure 16: Maps of monthly mean deposition velocities of SO_2 [original and modified Erisman (mE) scheme], NO_2 and HNO_3 for January (maps in the upper row) and June 1998 (maps in the lower row) in cm/s (color bar to the right of each map). The deposition velocities are valid at a height of 1.5 m.

In June the deposition velocities are generally larger than in January. Comparing the monthly mean values of v_d for the three components it should be noted that the dry deposition velocity of NO_2 is on the order of $10^{-3}\,ms^{-1}$ while the magnitude of v_d for SO_2 and HNO_3 is $10^{-2}\,ms^{-1}$. With the lower boundary of $r_{ext} = 10\,sm^{-1}$ the simulated v_d values for SO_2 are slightly smaller than those obtained with the original scheme of Erisman et al. (1994).

Sometimes, average values of the deposition velocity are needed, and an explicit variation of v_d with the actual meteorological conditions is not considered. The diagrams in Figure 17 and Figure 18 show mean v_d values of four species for all land use classes. The values are means over the deposition velocities simulated for the period of one month (with a resolution of 3 h, i.e. about 240 values per month) in the complete model domain (about 12000 grid points). Therefore, they represent mean values of v_d encountered under a relatively large variety of meteorological conditions. Note that these values are not weighted with the actual fractional area coverage of the classes.

For those land use classes where a seasonal cycle is considered, maximum deposition velocities are present during summer. In the case of the particle species Ca^{2+} (Figure 17) this is directly due to the difference of the roughness length accounted for in the computation of r_a and the setting of r_b. For land use classes without a seasonal cycle (e.g. spruce/pine, urban), the month to month variation of the averaged deposition velocity is negligible, resulting only from differences in the relevant meteorological conditions encountered during the months.

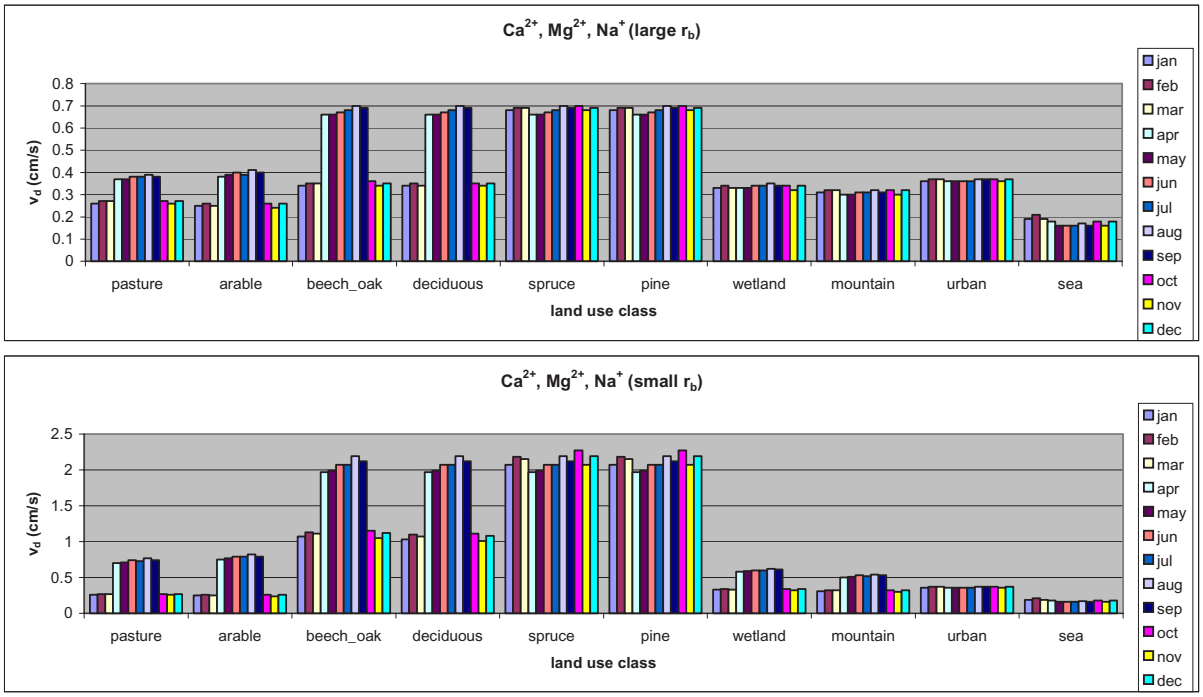

Figure 17: Monthly mean deposition velocities of Ca^{2+} for the different land use classes, averaged over the MATCH-Sweden domain. Upper panel: simulation with large r_b (settings as in Table 2); lower panel: small r_b (Table 3).

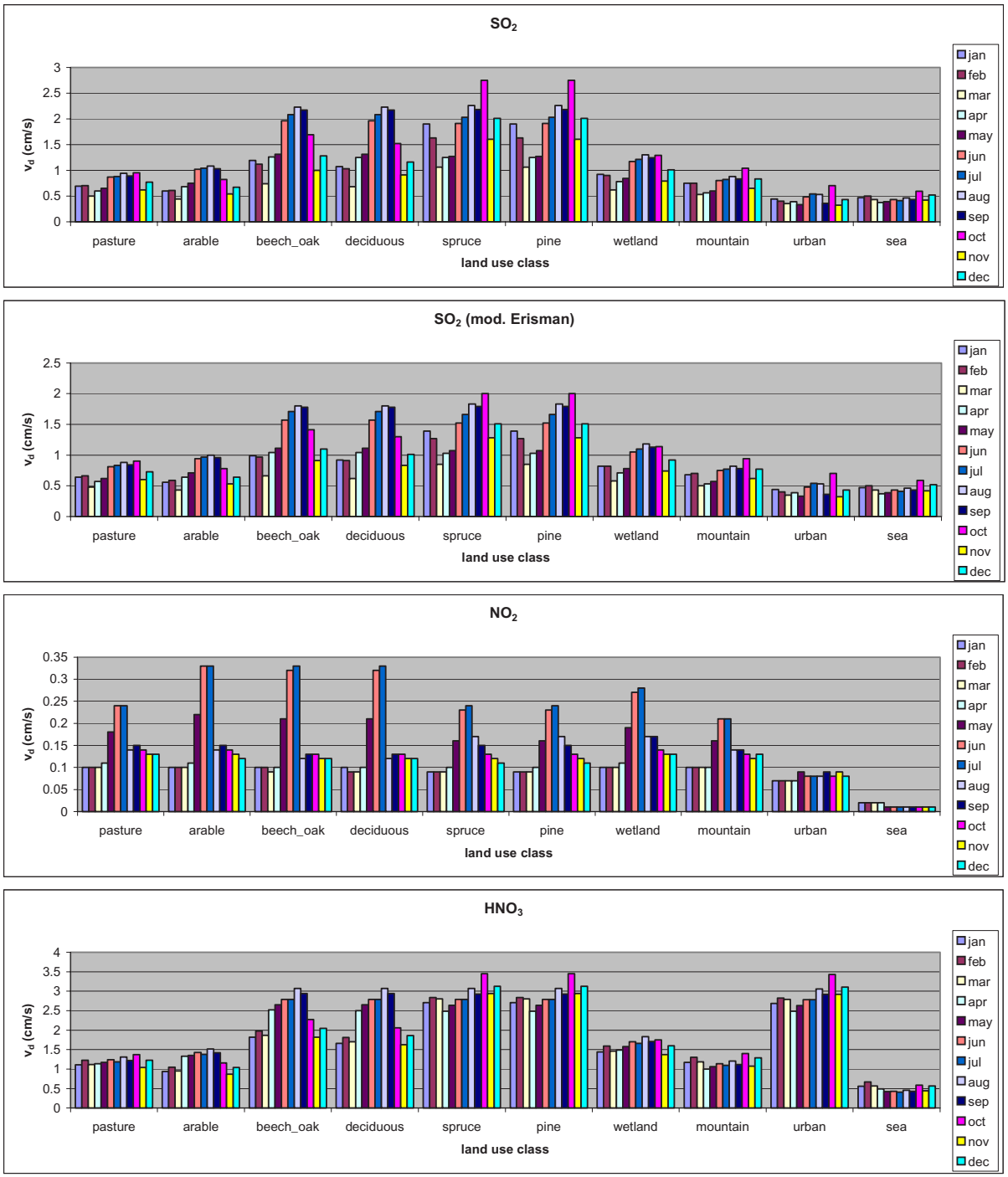

Figure 18: Same as Figure 17, but for SO_2, (control run and run with modified Erisman scheme), NO_2 and HNO_3 (from top to bottom).

For SO_2, NO_2 and HNO_3 (Figure 18) both r_a and r_b depend on the friction velocity and thus on the roughness height z_0. As pointed out before, the calculation of v_d is significantly more complicated for gases, since the variation of the surface resistance r_s is determined by a number of different parameters and variables. For SO_2 the external resistance dominates the surface resistance, providing an efficient deposition mechanism throughout the year. For NO_2, however, stomata uptake is more important. Thus, for all vegetation classes the maximum

deposition velocities occur during the summer months June and July. Since no stomata uptake of HNO_3 is considered in the parameterization, the maximum dry deposition velocities occur over the land use classes with the largest surface roughness. Additional average deposition velocities of other components are given in Appendix B.

The presented average values of v_d are well within the spectrum of dry deposition literature values, e.g. the overview presented by Davidson and Wu (1989). Yet, considering the range of the latter spectrum, the range of uncertainties becomes clear. Thus, a detailed validation of the dry deposition scheme will probably require a number of case studies covered by both modeling and measurements. At present it can therefore be stated that the calculated values are physically reasonable, although they might be subject to changes in the future as a result of changes in the individual settings and calculations of the different partial resistances.

Figure 19 shows the horizontal distribution of $v_{d,l}$ of SO_2 (modified Erisman scheme weighted with the fractional area coverage of the respective class α_l and normalized by the total deposition velocity v_d in %. Therefore, the shown quantity reflects both the distribution of the individual classes α_l (see also Figure 2) and the modeled deposition velocities for these classes, i.e. it provides a measure of how many percent of the value of v_d are accounted for by each class.

The largest contributions to v_d are provided by the classes spruce and pine over most continental areas apart from the mountain regions in northern Norway and Sweden, where the classes mountain and also deciduous (in regions adjacent to the mountain range) dominate.

The importance of the stomata resistance for the deposition of SO_2 and NO_2 can be seen from Figure 20, where the differences between the control run with full dry deposition parameterization and the sensitivity run with the stomata uptake switched off are displayed. For SO_2 the differences are generally relatively small on the order of a few % of v_d in the control run. Maximum differences with up to 20% occur in the vicinity of the northern Scandinavian mountain range. This reflects the comparably large percentage of deciduous in that area, for which the stomata resistance was shown to be especially important (see Section 3.1.6). In addition, the monthly-mean relative humidity is comparatively low in that area (not shown) which leads to relatively small external leaf uptake of SO_2 and thus larger importance of stomata uptake.

For NO_2 the stomata uptake of pollutants plays a very important role (Figure 20). Over a large part of Scandinavia stomata uptake accounts for about 50% to 60% of the deposition velocity during June 1998. This is a consequence of the relatively low deposition to the external of plants compared to SO_2, for which the deposition process is dominated by r_{ext} and changes in r_{stom} thus have a smaller relative impact. For NO_2 a good description of the stomata uptake of plants is consequently of great importance.

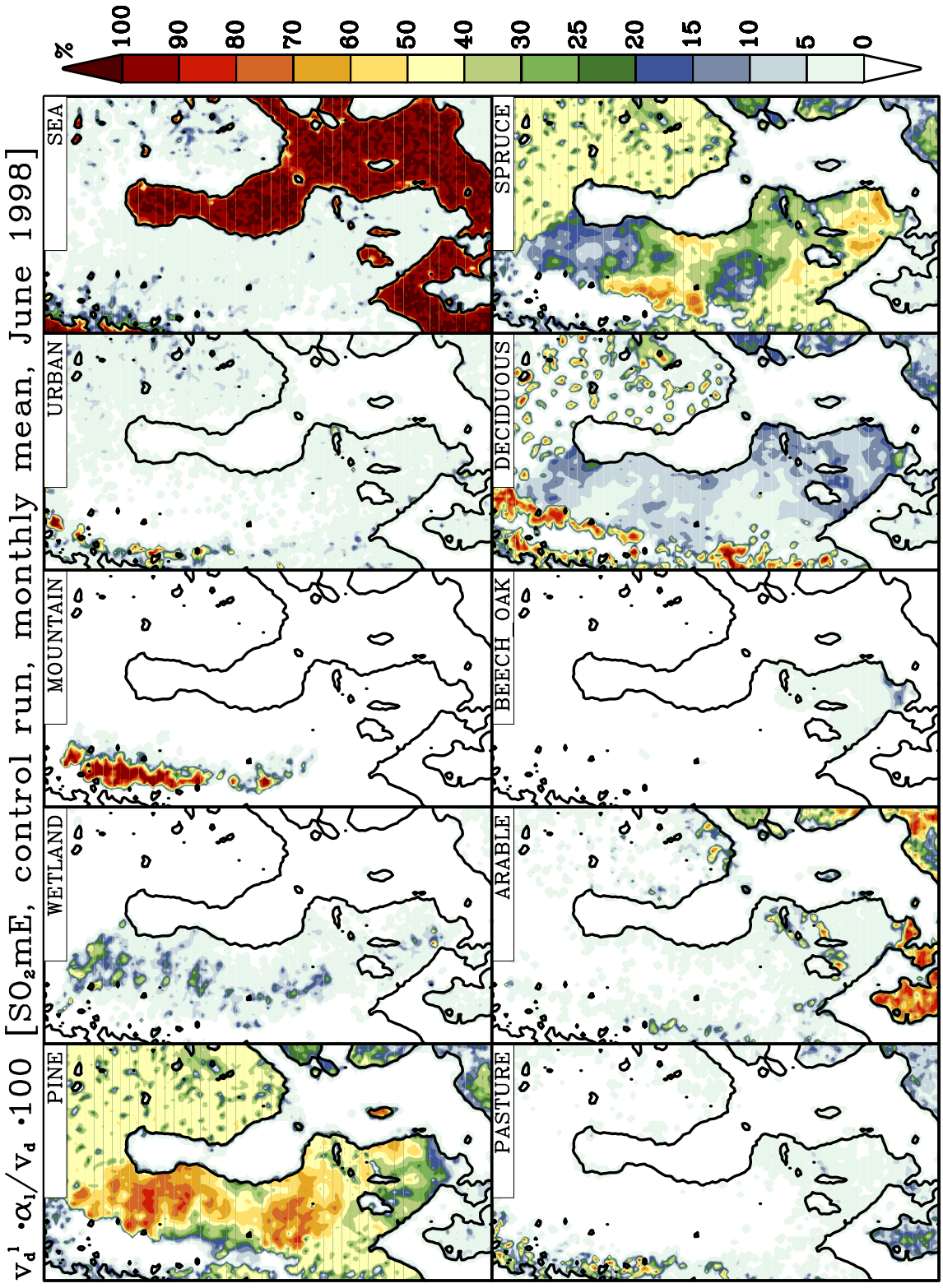

Figure 19: MATCH-modeled dry deposition velocities of SO_2 (modified Erisman parameterization) in June 1998 (color bar to the right, in %) for the different land use classes (lower panel from left to right: pasture, arable, beech/oak, deciduous, spruce; upper panel: pine, wetland, mountain, urban, sea). The velocities are weighted with the fractional area coverage of the respective land use class (i.e. the percentage of the class divided by 100) and normalized by the total deposition velocity v_d.

It becomes clear from the performed studies that the dry deposition of pollutants represents a process of extraordinary complexity that can only partially be accounted for in parameterizations. Despite the physical consistence and elegance of parameterizations such as the resistance concept the spectrum of results strongly depends on a number of initial assumptions and settings of parameters in equations which might only be valid for a special experiment and certain boundary conditions (e.g. meteorology, local surface characteristics). Yet, such a type of parameterization represents the state of the art in dry deposition modeling, and scientific efforts will have to continue to both gather experimental data of dry deposition processes while at the same time work on the improvement of the parameterization and the interdependence of the processes.

Modeled dry deposition maps for 1998 and Sweden (based on the parameterizations described in this report) can be found on SMHI's homepage (www.smhi.se → "Klimat & Miljö" → "Atmosfärskemi").

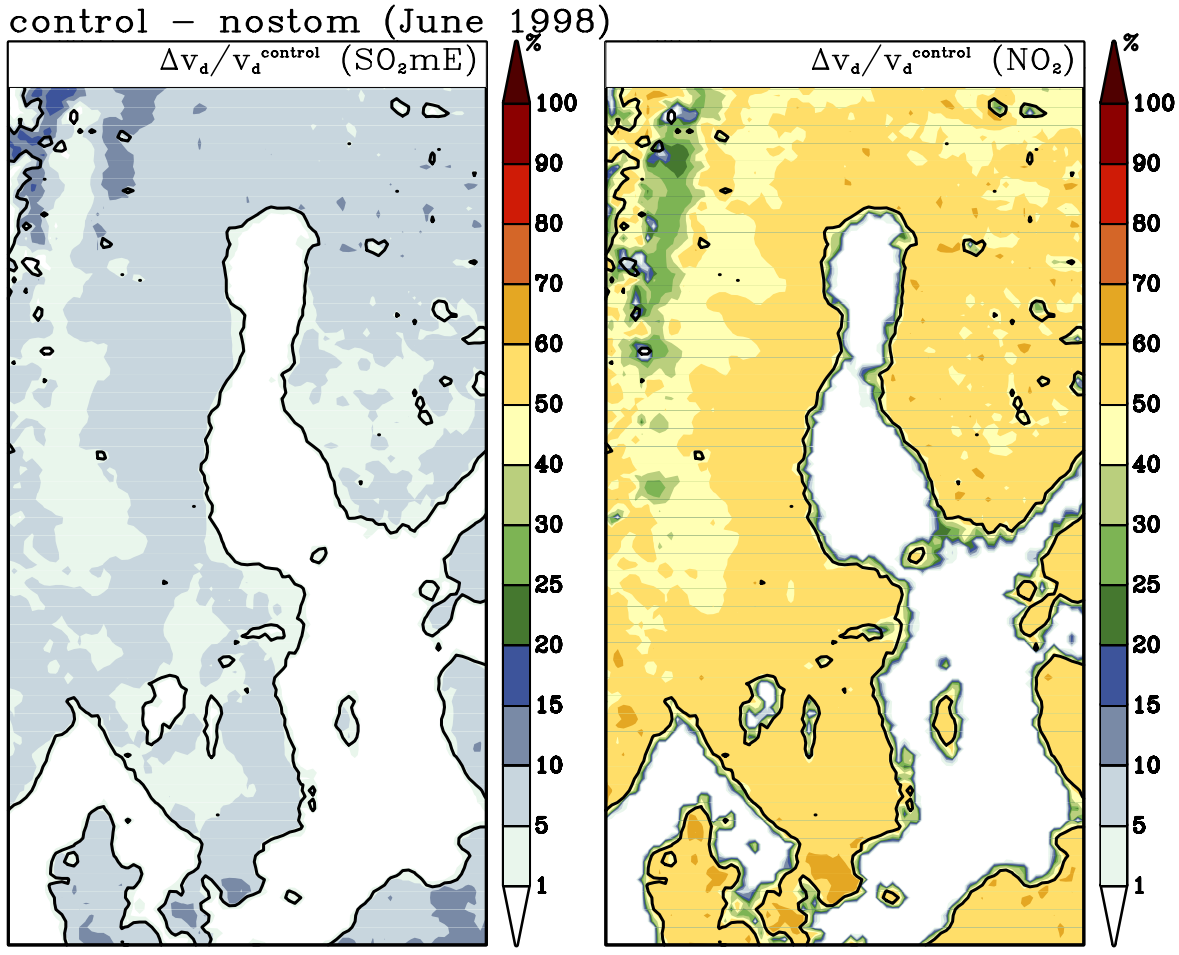

Figure 20: Differences between a control run with full deposition parameterization and a run without stomata uptake of pollutants for the species SO_2 (with modified Erisman scheme) and NO_2 in % of v_d of the control run.

4 Conclusions

The description of the dry deposition of pollutants from the atmosphere to the ground represents a key factor for the assessment of the state of the environment and subsequent ecological and economical decisions. A common approach to describe dry deposition both qualitatively and quantitatively is the resistance concept. Simulations of dry deposition velocities over Sweden have been performed using the MATCH model as operated at SMHI for environmental monitoring. The general principle of the resistance concept as well as problems and possible limitations of the parameterizations are described by means of time series of the dry deposition velocity under a variety of meteorological conditions and for different surface types and species.

For particles, the deposition velocity only depends on the variable aerodynamic resistance and the constant viscous sub-layer resistance and gravitational settling. The deposition velocity of gases is treated in a more sophisticated manner, depending largely on the actual meteorological situation and on the complex interplay of several partial resistances. For SO_2 the deposition is critically depending on the external resistance which varies strongly with relative humidity. A possible overestimation of the latter quantity by weather prediction models, which normally provide the meteorological input to the MATCH simulations, could consequently result in a significant overestimation of the SO_2 deposition. The strong dependence of the SO_2 deposition on the external resistance implies a comparably low (but not negligible) impact of the stomata uptake of plants for this species. A sensitivity study with the stomata uptake switched off shows that deposition to the stomata of plants accounts for up to 20% of the total deposition of SO_2 and up to 70% of NO_2 in Sweden during summer. For NO_2 stomata uptake is very important since both the external resistance and the soil resistance of NO_2 are relatively large.

The description of dry deposition in the model could probably be further improved by the incorporation of some additional effects. The following tasks seem to be of major importance:

- A better description of the laminar sub-layer resistance of particles (see also Appendix A).
- A more sophisticated regional and time-dependent description of the in-canopy resistance of gases using detailed maps (e.g. remote sensing products) of the leaf-area index.
- A better description of the soil resistance by including the pH of soil and precipitation.
- Incorporation of surface water content in the computation of the stomata resistance.
- Assuring a high quality and accuracy of driving parameters and data, e.g. land use classification and surface roughness maps and meteorological data.

In addition, a considerable improvement of the description of dry deposition would very probably result from a further intensification of experimental efforts to provide data available for both the derivation of new parameterizations and the validation of existing ones.

Mean values for each month of the year 1998 and a number of chemical species were derived for all surface class-specific deposition velocities. These values are averages in space and time and, thus, represent means over a large spectrum of different meteorological conditions during the respective month. Therefore, they can be used as average values for deposition modeling in studies, where no explicit calculation of the dry deposition velocity can be performed. The means presented are based only on meteorological data of 1998. Future studies at SMHI will also investigate data of other years and examine the yearly variation of v_d. A change in the mean meteorological conditions can be expected to have an impact on dry deposition. E.g., a warmer climate could directly (near surface temperature) or indirectly (associated changes in cloudiness / radiation) imply modifications of the pollutant deposition to the stomata of plants. Changes in the mean near surface wind speed or precipitation associated with altered atmospheric circulation patterns are also likely to lead to changes in pollutant deposition patterns.

References

Bartnicki, J, Olendrzynski, K, Jonson, J. E., Berge, E., and Unger, S., 2001: Description of the Eulerian acid deposition model. http://projects.dnmi.no/~emep/acid/eudm.pdf

Berkowicz, R., Olesen, H. R., and Torp, U., 1986: The Danish Gaussian air pollution model (OML): Description, test and sensitivity analysis in view of regulatory applications. In Proceedings of the 15th NATO/CCMS International Technical Meeting on Air Pollution Modelling and Its Application. Plenum Press, New York, 453-481.

Bott, A., 1989a: A positive definite advection scheme obtained by non-linear renormalization of advective fluxes. *Monthly Weather Rev.,* **117,** 1006-1015.

Bott, A., 1989b: Reply. *Monthly Weather Rev.,* **117,** 2633-2636.

Bott, A., 1992: Monotone flux limitation in the area preserving flux-form advection algorithm. *Monthly Weather Rev.,* **120,** 2592-2602.

Chamberlain, A. C. and Chadwick, R. C., 1965: Transport of iodine from atmosphere to ground. *Tellus,* **18,** 226-237.

Davidson, C. I., and Wu, Y. L., 1989: Dry deposition of particles and vapors. In Acid Precipitation, Vol. 3, edited by S. E. Lindberg, A. L. Page, and S. A. Norton. Springer-Verlag, Berlin, 103-209.

Erisman, J. W., Van Pul, A., and Wyers, P., 1994: Parametrization of surface resistance for the quantification of atmospheric deposition of acidifying pollutants and ozone. *Atmospheric Environment,* **25,** 2595-2607.

Garland, J. A., 1978: Dry and wet removal of sulfur from the atmosphere. *Atmospheric Environment,* **12,** 349-362.

Hicks, B. B., Baldocchi, D. D., Hosker, R. P. Jr., Hutchinson, T. A., Matt, D. R., McMillen, R. T., and Satterfield, L. C., 1985: On the use of monitored air concentrations to infer dry deposition. NOAA Technical Memorandum ERL ARL-141, Silver Spring, MD.

Hicks, B. B., Baldocchi, D. D., Mayers, T. P., Hosker, R. P. Jr., and Matt, D. R., 1987: A preliminary multiple resistance routine for deriving dry deposition velocities from measured quantities. *Water, Air and Soil Pollution,* **36,** 311-330.

Hicks, B. B., and Liss, P. S., 1976: Transfer of SO_2 and other reactive gases across the air-sea interface. *Tellus,* **36,** 311-330.

Holtslag, A. A. M., Meijgard, E., and De Rooy, W. C., 1995: A comparison of boundary layer diffusion schemes in unstable conditions over land. *Boundary-Layer Met.,* **76,** 69-95.

Häggmark, L., Ivarsson, K.-I., Gollvik, S., and Olofsson, P.-O., 2000: Mesan, an operational mesoscale analysis system. *Tellus,* **52,** 2-20.

Jakobsen, H. A., Jonson, J. E., and Berge, E., 1996: Transport and deposition calculations of sulphur and nitrogen compounds in Europe for 1992 in the 50 km grid by use of the multi-layer Eulerian model. EMEP MSC-W Note 2/96. The Norwegian Meteorological Institute, Oslo, Norway.

Jonson, J. E., and Berge, E., 1995: Some preliminary results on transport and deposition of nitrogen compounds by use of the multilayer Eulerian model. EMEP/MSC-W Note 1/95. The Norwegian Meteorological Institute, Oslo, Norway.

Josefsson, W., 1989: Computed global radiation using interpolated, gridded cloudiness from the meso-beta analysis compared to measured global radiation. Reports Meteorology, No. 101. Swedish Meteorological and Hydrological Institute, Norrköping, Sweden.

Källén, E., 1996: HIRLAM documentation manual, System 2.5. Swedish Meteorological and Hydrological Institute, Norrköping, Sweden.

Langner, J., Bergström, R., and Pleijel, K., 1998: European scale modeling of sulfur, oxidized nitrogen and photochemical oxidants. Model development and evaluation for the 1994 growing season. Reports Meteorology and Climatology, No. 82. Swedish Meteorological and Hydrological Institute, Norrköping, Sweden.

Persson, C, Langner J., and Robertson L., 1996: Air pollution assessment studies for Sweden based on the MATCH model and air pollution measurements. Air Pollution Modeling and Its Application XI, edited by Gryning and Schiermeier, Plenum Press, New York.

Persson, C., Lövblad, G., and Roos, E., 2000: Meso-scale modelling of base cation deposition in Sweden. Air Pollution Modeling and Its Application XI, edited by S.-E. Gryning and E. Batchvarova, Kluwer Academic/Plenum Publishers.

Robertson, L., Langner, J., and Engardt, M., 1999. An Eulerian limited-area atmospheric transport model. *J. Appl. Meteor.,* **38,** 190-210.

Seinfeld, J. H., and Pandis, S. N., 1997: Atmospheric Chemistry and Physics: From Air Pollution to Global Change. John Wiley and Sons, New York.

Tørseth, K., and Semb, A., 1998: Deposition of nitrogen and other major inorganic compounds in Norway, 1992-1996. *Environmental Pollution,* **102,** S1, 299-304.

Van Pul, W. A. J., and Jacobs, A. F. G., 1994: The conductance of a maize crop and the underlying soil to ozone under various environmental conditions. *Boundary-Layer Met.,* **69,** 83-99.

Wesley, M. L., 1989: Parameterization of surface resistances to gaseous dry deposition in regional-scale numerical models. *Atmospheric Environment,* **23,** 1293-1304.

Zhang, L., Gong, S., Padro, J., and Barrie, L., 2001: A size-segregated particle deposition scheme for an atmospheric aerosol module. *Atmospheric Environment,* **35,** 549-560.

Appendix

A. Alternative computation of r_b

Recently, more sophisticated computations of the laminar sub-layer resistance r_b of particles have been tested in MATCH. Most parameterizations are generally obtained from measurements under relatively short periods of time covering only part of the range of meteorological conditions encountered during longer periods or in regions other than the place of the experiments. For larger values of u_*, e.g., unrealistically large dry deposition velocities were obtained for some schemes tested in MATCH. A recent overview over dry deposition schemes for particles can be found in Zhang et al. (2001). The following scheme for r_b proposed by Zhang et al. (2001) is currently tested in MATCH:

$$r_b = \frac{1}{\varepsilon_0 u_* (E_B + E_{IM} + E_{IN}) R_1},$$

where E_B, E_{IM} and E_{IN} are the collection efficiency from Brownian diffusion, impaction and interception, respectively. ε_0 represents an empirical constant taken as 3 for all land use classes, and R_1 is a correction factor representing the fraction of particles that stick to the surface. Zhang et al. (2001) use the following formulae for E_B, E_{IM} and E_{IN}, respectively:

$E_B = Sc^{-\gamma}$, where Sc is the Schmidt number and γ a coefficient varying with land use classes;

$E_{IM} = \left(\frac{St}{\alpha + St} \right)^{\beta}$, where St denotes the Stokes number, β is taken as 2 and α varies with land use category;

$E_{IN} = \frac{1}{2} \left(\frac{d_p}{A} \right)^2$, where d_p is the particle diameter and A is a characteristic radius, which depends on land use class and seasonal category.

$R_1 = \exp(-St^{1/2})$ accounts for the rebound of large particles with the limitation that no rebound occurs from wet surfaces.

The Stokes number is calculated as $St = \frac{v_s u_*}{g A}$ for vegetated surfaces and as $St = \frac{v_s u_*^2}{\nu}$ for smooth surfaces or surfaces with bluff roughness elements.

At present, the settings proposed by Zhang et al. (2001) are used in MATCH for the land use class-specific parameters.

B. Additional deposition velocities

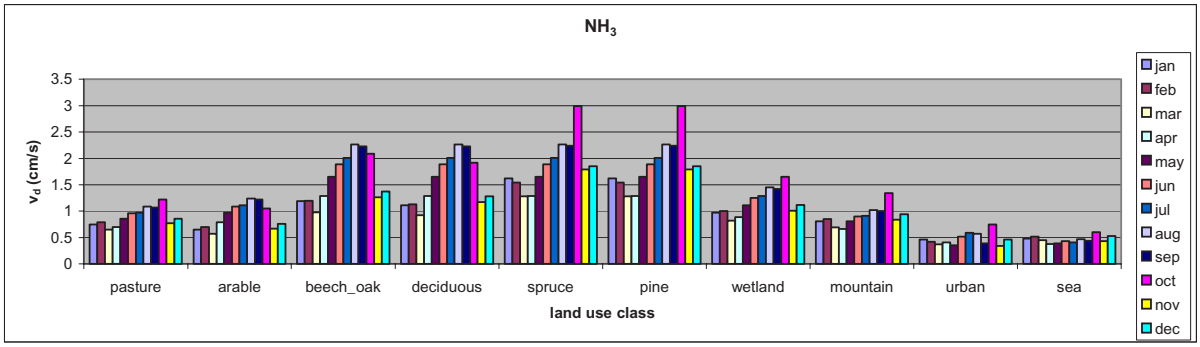

Figure 21 Monthly mean deposition velocities of NH_3 for the different land use classes, averaged over the MATCH-Sweden domain.

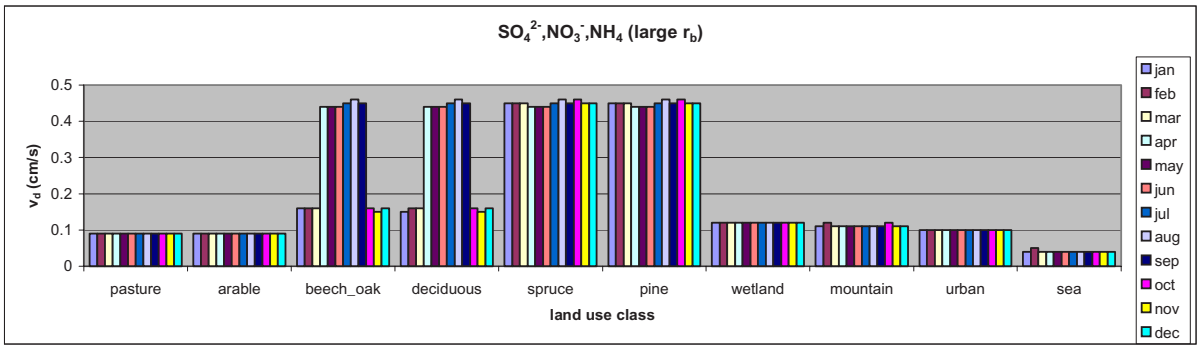

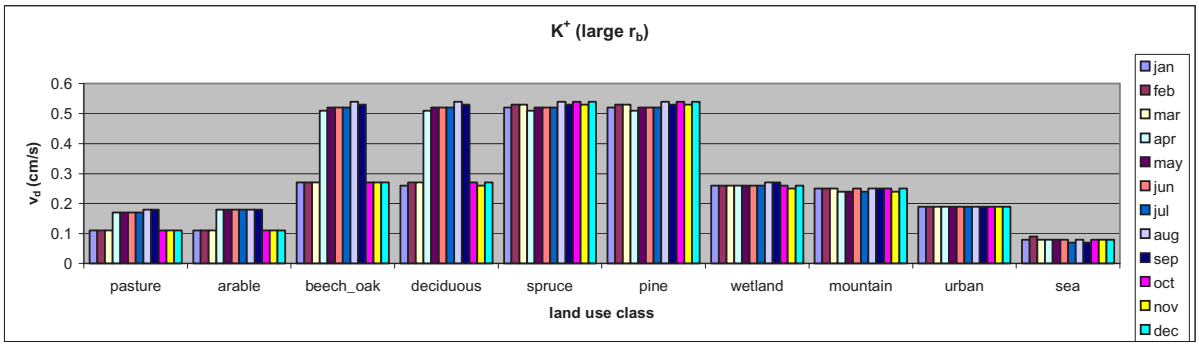

Figure 22: Same as Figure 21, but for SO_4^{2-} / NO_3^- / NH_4 and K^+ (large r_b, Table 2).

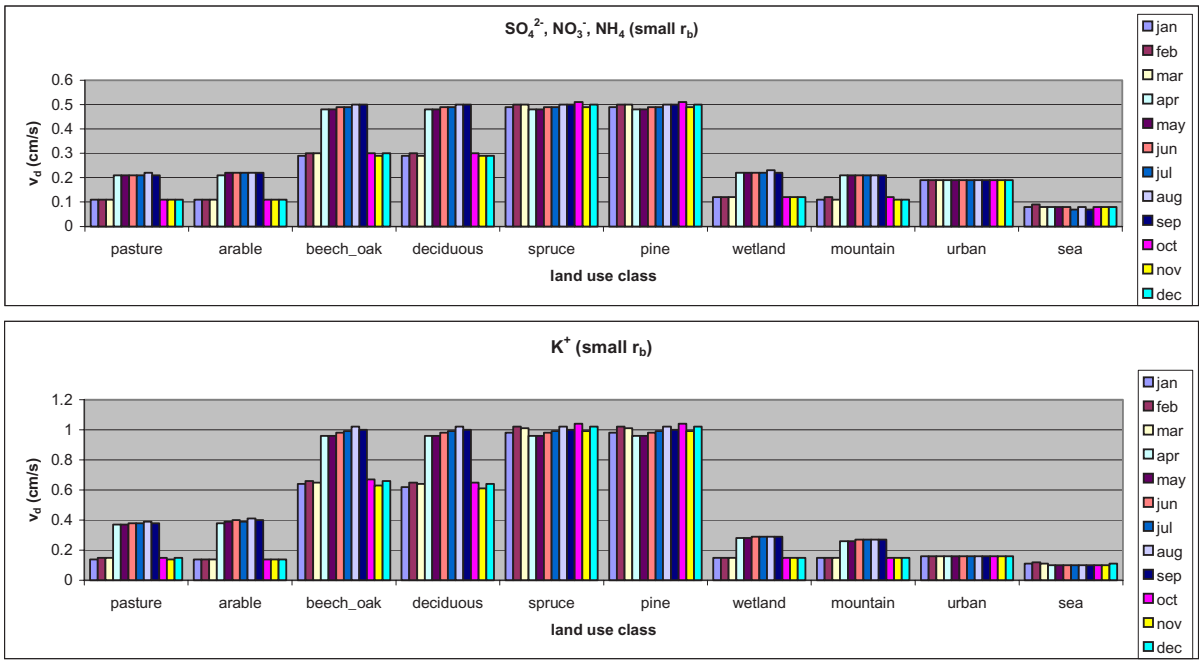

Figure 23: Same as Figure 21, but for SO_4^{2-} / NO_3^- / NH_4 and K^+ (small r_b , Table 3).

SMHIs publications

SMHI publishes six report series. Three of these, the R-series, are intended for international readers and are in most cases written in English. For the others the Swedish language is used.

Names of the Series	**Published since**
RMK (Report Meteorology and Climatology)	1974
RH (Report Hydrology)	1990
RO (Report Oceanography)	1986
METEOROLOGI	1985
HYDROLOGI	1985
OCEANOGRAFI	1985

Earlier issues published in serie RMK

1 Thompson, T., Udin, I., and Omstedt, A. (1974)
Sea surface temperatures in waters surrounding Sweden.

2 Bodin, S. (1974)
Development on an unsteady atmospheric boundary layer model.

3 Moen, L. (1975)
A multi-level quasi-geostrophic model for short range weather predictions.

4 Holmström, I. (1976)
Optimization of atmospheric models.

5 Collins, W.G. (1976)
A parameterization model for calculation of vertical fluxes of momentum due to terrain induced gravity waves.

6 Nyberg, A. (1976)
On transport of sulphur over the North Atlantic.

7 Lundqvist, J.-E., and Udin, I. (1977)
Ice accretion on ships with special emphasis on Baltic conditions.

8 Eriksson, B. (1977)
Den dagliga och årliga variationen av temperatur, fuktighet och vindhastighet vid några orter i Sverige.

9 Holmström, I., and Stokes, J. (1978)
Statistical forecasting of sea level changes in the Baltic.

10 Omstedt, A., and Sahlberg, J. (1978)
Some results from a joint Swedish-Finnish sea ice experiment, March, 1977.

11 Haag, T. (1978)
Byggnadsindustrins väderberoende, seminarieuppsats i företagsekonomi, B-nivå.

12 Eriksson, B. (1978)
Vegetationsperioden i Sverige beräknad från temperaturobservationer.

13 Bodin, S. (1979)
En numerisk prognosmodell för det atmosfäriska gränsskiktet, grundad på den turbulenta energiekvationen.

14 Eriksson, B. (1979)
Temperaturfluktuationer under senaste 100 åren.

15 Udin, I., och Mattisson, I. (1979)
Havsis- och snöinformation ur datorbearbetade satellitdata - en modellstudie.

16 Eriksson, B. (1979)
Statistisk analys av nederbördsdata. Del I. Arealnederbörd.

17 Eriksson, B. (1980)
Statistisk analys av nederbördsdata. Del II. Frekvensanalys av månadsnederbörd.

18 Eriksson, B. (1980)
Årsmedelvärden (1931-60) av nederbörd, avdunstning och avrinning.

19 Omstedt, A. (1980)
A sensitivity analysis of steady, free floating ice.

20 Persson, C., och Omstedt, G. (1980)
En modell för beräkning av luftföroreningars spridning och deposition på mesoskala.

21 Jansson, D. (1980)
Studier av temperaturinversioner och vertikal vindskjuvning vid Sundsvall-Härnösands flygplats.

22 Sahlberg, J., and Törnevik, H. (1980)
A study of large scale cooling in the Bay of Bothnia.

23 Ericson, K., and Hårsmar, P.-O. (1980)
Boundary layer measurements at Klock-rike. Oct. 1977.

24 Bringfelt, B. (1980)
A comparison of forest evapotranspiration determined by some independent methods.

25 Bodin, S., and Fredriksson, U. (1980)
Uncertainty in wind forecasting for wind power networks.

26 Eriksson, B. (1980)
Graddagsstatistik för Sverige.

27 Eriksson, B.(1981)
Statistisk analys av nederbördsdata. Del III. 200-åriga nederbördsserier.

28 Eriksson, B. (1981)
Den "potentiella" evapotranspirationen i Sverige.

29 Pershagen, H. (1981)
Maximisnödjup i Sverige (perioden 1905-70).

30 Lönnqvist, O. (1981)
Nederbördsstatistik med praktiska tillämpningar.
(Precipitation statistics with practical applications.)

31 Melgarejo, J.W. (1981)
Similarity theory and resistance laws for the atmospheric boundary layer.

32 Liljas, E. (1981)
Analys av moln och nederbörd genom automatisk klassning av AVHRR-data.

33 Ericson, K. (1982)
Atmospheric boundary layer field experiment in Sweden 1980, GOTEX II, part I.

34 Schoeffler, P. (1982)
Dissipation, dispersion and stability of numerical schemes for advection and diffusion.

35 Undén, P. (1982)
The Swedish Limited Area Model. Part A. Formulation.

36 Bringfelt, B. (1982)
A forest evapotranspiration model using synoptic data.

37 Omstedt, G. (1982)
Spridning av luftförorening från skorsten i konvektiva gränsskikt.

38 Törnevik, H. (1982)
An aerobiological model for operational forecasts of pollen concentration in the air.

39 Eriksson, B. (1982)
Data rörande Sveriges temperaturklimat.

40 Omstedt, G. (1984)
An operational air pollution model using routine meteorological data.

41 Persson, C., and Funkquist, L. (1984)
Local scale plume model for nitrogen oxides. Model description.

42 Gollvik, S. (1984)
Estimation of orographic precipitation by dynamical interpretation of synoptic model data.

43 Lönnqvist, O. (1984)
Congression - A fast regression technique with a great number of functions of all predictors.

44 Laurin, S. (1984)
Population exposure to SO and NO_x from different sources in Stockholm.

45 Svensson, J. (1985)
Remote sensing of atmospheric tempera-ture profiles by TIROS Operational Vertical Sounder.

46 Eriksson, B. (1986)
Nederbörds- och humiditetsklimat i Sverige under vegetationsperioden.

47 Taesler, R. (1986)
Köldperioden av olika längd och förekomst.

48 Wu Zengmao (1986)
Numerical study of lake-land breeze over Lake Vättern, Sweden.

49 Wu Zengmao (1986)
Numerical analysis of initialization procedure in a two-dimensional lake breeze model.

50 Persson, C. (1986)
Local scale plume model for nitrogen oxides. Verification.

51 Melgarejo, J.W. (1986)
An analytical model of the boundary layer above sloping terrain with an application to observations in Antarctica.

52 Bringfelt, B. (1986)
Test of a forest evapotranspiration model.

53 Josefsson, W. (1986)
Solar ultraviolet radiation in Sweden.

54 Dahlström, B. (1986)
Determination of areal precipitation for the Baltic Sea.

55 Persson, C. (SMHI), Rodhe, H. (MISU), De Geer, L.-E. (FOA) (1986)
The Chernobyl accident - A meteorological analysis of how radionucleides reached Sweden.

56 Persson, C., Robertson, L. (SMHI), Grennfelt, P., Kindbom, K., Lövblad, G., och Svanberg, P.-A. (IVL) (1987)
Luftföroreningsepisoden över södra Sverige 2 - 4 februari 1987.

57 Omstedt, G. (1988)
An operational air pollution model.

58 Alexandersson, H., Eriksson, B. (1989)
Climate fluctuations in Sweden 1860 - 1987.

59 Eriksson, B. (1989)
Snödjupsförhållanden i Sverige - Säsongerna 1950/51 - 1979/80.

60 Omstedt, G., Szegö, J. (1990)
Människors exponering för luftföroreningar.

61 Mueller, L., Robertson, L., Andersson, E., Gustafsson, N. (1990)
Meso-γ scale objective analysis of near surface temperature, humidity and wind, and its application in air pollution modelling.

62 Andersson, T., Mattisson, I. (1991)
A field test of thermometer screens.

63 Alexandersson, H., Gollvik, S., Meuller, L. (1991)
An energy balance model for prediction of surface temperatures.

64 Alexandersson, H., Dahlström, B. (1992)
Future climate in the Nordic region - survey and synthesis for the next century.

65 Persson, C., Langner, J., Robertson, L. (1994)
Regional spridningsmodell för Göteborgs och Bohus, Hallands och Älvsborgs län. (A mesoscale air pollution dispersion model for the Swedish west-coast region. In Swedish with captions also in English.)

66 Karlsson, K.-G. (1994)
Satellite-estimated cloudiness from NOAA AVHRR data in the Nordic area during 1993.

67 Karlsson, K-G. (1996)
Cloud classifications with the SCANDIA model.

68 Persson, C., Ullerstig, A. (1996)
Model calculations of dispersion of lindane over Europe. Pilot study with comparisons to measurements around the Baltic Sea and the Kattegat.

69 Langner, J., Persson, C., Robertson, L., and Ullerstig, A. (1996)
Air pollution Assessment Study Using the MATCH Modelling System. Application to sulfur and nitrogen compounds over Sweden 1994.

70 Robertson, L., Langner, J., Engardt, M. (1996)
MATCH - Meso-scale Atmosperic Transport and Chemistry modelling system.

71 Josefsson, W. (1996)
Five years of solar UV-radiation monitoring in Sweden.

72 Persson, C., Ullerstig, A., Robertson, L., Kindbom, K., Sjöberg, K. (1996)
The Swedish Precipitation Chemistry Network. Studies in network design using the MATCH modelling system and statistical methods.

73 Robertson, L. (1996)
Modelling of anthropogenic sulfur deposition to the African and South American continents.

74 Josefsson, W. (1996)
Solar UV-radiation monitoring 1996.

75 Häggmark, L., Ivarsson, K.-I. (SMHI), Olofsson, P.-O. (Militära vädertjänsten). (1997)
MESAN - Mesoskalig analys.

76 Bringfelt, B, Backström, H, Kindell, S, Omstedt, G, Persson, C, Ullerstig, A. (1997)
Calculations of PM-10 concentrations in Swedish cities- Modelling of inhalable particles

77 Gollvik, S. (1997)
The Teleflood project, estimation of precipitation over drainage basins.

78 Persson, C., Ullerstig, A. (1997)
Regional luftmiljöanalys för Västmanlands län baserad på MATCH modell-beräkningar och mätdata - Analys av 1994 års data

79 Josefsson, W., Karlsson, J.-E. (1997)
Measurements of total ozone 1994-1996.

80 Rummukainen, M. (1997)
Methods for statistical downscaling of GCM simulations.

81 Persson, T. (1997)
Solar irradiance modelling using satellite retrieved cloudiness - A pilot study

82 Langner, J., Bergström, R. (SMHI) and Pleijel, K. (IVL) (1998)
European scale modelling of sulfur, oxidized nitrogen and photochemical oxidants. Model development and evaluation for the 1994 growing season.

83 Rummukainen, M., Räisänen, J., Ullerstig, A., Bringfelt, B., Hansson, U., Graham, P., Willén, U. (1998)
RCA - Rossby Centre regional Atmospheric climate model: model description and results from the first multi-year simulation.

84 Räisänen, J., Döscher, R. (1998)
Simulation of present-day climate in Northen Europé in the HadCM2 OAGCM.

85 Räisänen, J., Rummukainen, M., Ullerstig, A., Bringfelt, B., Ulf Hansson, U., Willén, U. (1999)
The First Rossby Centre Regional Climate Scenario - Dynamical Downscaling of CO_2-induced Climate Change in the HadCM2 GCM.

86 Rummukainen, Markku. (1999)
On the Climate Change debate

87 Räisänen, Jouni (2000)
CO_2-induced climate change in northern Europé: comparison of 12 CMIP2 experiments.

88 Engardt, Magnuz (2000)
Sulphur simulations for East Asia using the MATCH model with meteorological data from ECMWF.

89 Persson, Thomas (2000)
Measurements of Solar Radiation in Sweden 1983-1998

90 Daniel B. Michelson, Tage Andersson Swedish Meteorological and Hydrological Institute (2000)
Jarmo Koistinen, Finnish Meteorological Institute
Christopher G. Collier, Telford Institute of Environmental Systems, University of Salford
Johann Riedl, German Weather Service
Jan Szturc, Instiute of Meteorology and Water Management
Uta Gjertsen, The Norwegian Meteorological Institute
Aage Nielsen, Danish Meteorological Institute
Søren Overgaard, Danish Meteorological Institute
BALTEX Radar Data Centre Products and their Methodologies

91 Josefsson, Weine (2000)
Measurements of total ozone 1997 – 1999

92 Andersson, Tage (2000)
Boundary clear air echos in southern Sweden

93 Andersson, Tage (2000)
Using the Sun to check some weather radar parameters

94 Rummukainen, M.,S. Bergström, E. Källén, L. Moen, J. Rodhe, M. Tjernström (2000)
SWECLIM – The First Three Years

95 Meier, H. E Markus (2001)
The first Rossby Centre regional climate scenario for the Baltic Sea using a 3D coupled ice-ocean model

96 Landelius, Tomas, Weine Josefsson, Thomas Persson (2001)
A system for modelling solar radiation parameters with mesoscale spatial resolution

97 Karlsson, Karl-Göran (2001)
A NOAA AVHRR cloud climatology over Scandinavia covering the period 1991-2000

98 Bringfelt, B., Räisänen, J., Gollvik, S., Lindström, G., Graham, P., Ullerstig, A., (2001)
The land surface treatment for the Rossby Centre Regional Atmospheric Climate Model - version 2 (RCA2)

99 Kauker, Frank , Alfred Wegener Institute for Polar and Marine Research, Germany and Meier, H.E. Markus, Swedish Meteorological and Hydrological Institute, Rossby Centre, Sweden (2002)
Reconstructing atmospheric surface data for the period 1902-1998 to force a coupled ocean-sea ice model of the Baltic Sea.

Swedish Meteorological and Hydrological Institute
SE 601 76 Norrköping, Sweden.
Tel +46 11-495 80 00. Fax +46 11-495 80 01

ISSN 0347-2116